Nucleic Acids Research, 2025, **53**, gkaf080
https://doi.org/10.1093/nar/gkaf080
Nucleic Acid Enzymes

Inter-domain communication in the dimeric DEAD-box helicase Hera from *T. thermophilus* and implications for the mechanism of RNA unwinding

Pascal Donsbach, Carolin Kwas, Lenz Steimer, Brighton Samatanga, Alexandra Z. Andreou, Dagmar Klostermeier*

University of Muenster, Institute for Physical Chemistry, Corrensstrasse 30, 48149 Muenster, Germany
*To whom correspondence should be addressed. Email: dagmar.klostermeier@uni-muenster.de

Abstract

The *Thermus thermophilus* DEAD-box helicase Hera consists of the conserved helicase core, followed by a dimerization domain (DD) and an RNA-binding domain (RBD). The RBD mediates high-affinity binding to an RNA hairpin; the DD mediates formation of a stable dimer. In the dimer, the active sites of the two helicase cores face each other in an ideal configuration to cooperate functionally in RNA unwinding. Here, we dissect the communication between the two RBDs and helicase cores by characterizing dimeric deletion variants with two cores, but two, one, or no RBDs, variants with both RBDs, but two, one, or no functional core, and variants with one core and one RBD, either on the same or opposite protomers. We show that RNA binds to Hera in a two-step mechanism, with an initial interaction between the RBD and a hairpin, followed by the interaction of the core with the flanking single- or double-stranded region. The duplex preferentially interacts with the core on the same protomer in the absence of ATP, but in the presence of ATP, interactions with the other core become possible. Overall, our results point to limited but significant cooperativity between the two protomers in RNA unwinding.

Graphical abstract

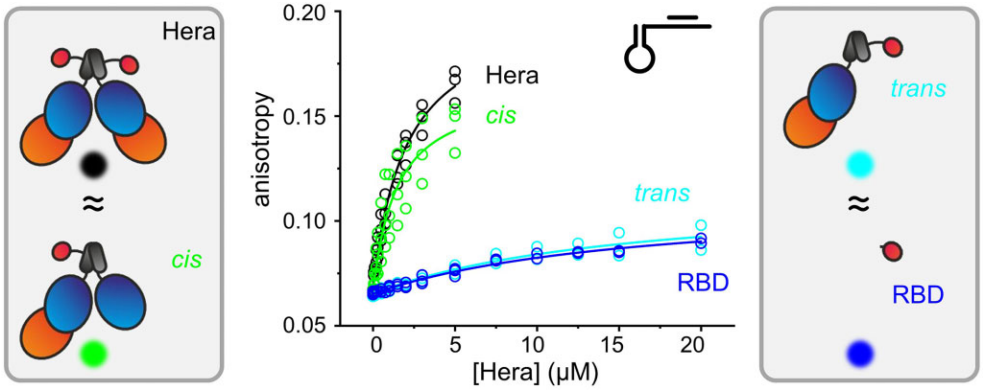

Introduction

RNA helicases of the DEAD-box family unwind RNA duplexes in an ATP-dependent reaction (reviewed in [1–3]). They share a common helicase core of two flexibly linked globular domains that carry the helicase signature motifs mediating ATP binding and hydrolysis, RNA binding, and duplex unwinding. In many representatives, additional domains flanking the core region affect nucleotide binding and hydrolysis, and contribute to RNA binding and specificity, or binding of protein partners [4–13], or to duplex destabilization [14] (recently reviewed in [1]).

Hera is a DEAD-box protein from *Thermus thermophilus* [15] (reviewed in [16]) that consists of a helicase core, followed by a bipartite C-terminal extension that contains a dimerization domain (DD) and an RNA-binding domain (RBD) [17–20] (Fig. 1A). The DD in Hera mediates the formation of a stable dimer [19], even at picomolar concentrations [8] (Fig. 1B). The RBD, attached to the DD by a short double-β-hairpin structure [17], consists of an RNA recognition motif (RRM) with a central four-stranded β-sheet flanked by an α-helix and a disordered C-terminal tail of ten amino acids [17]. The RBD mediates binding of Hera to RNAs containing

Received: August 29, 2024. **Revised:** January 20, 2025. **Editorial Decision:** January 24, 2025. **Accepted:** February 3, 2025

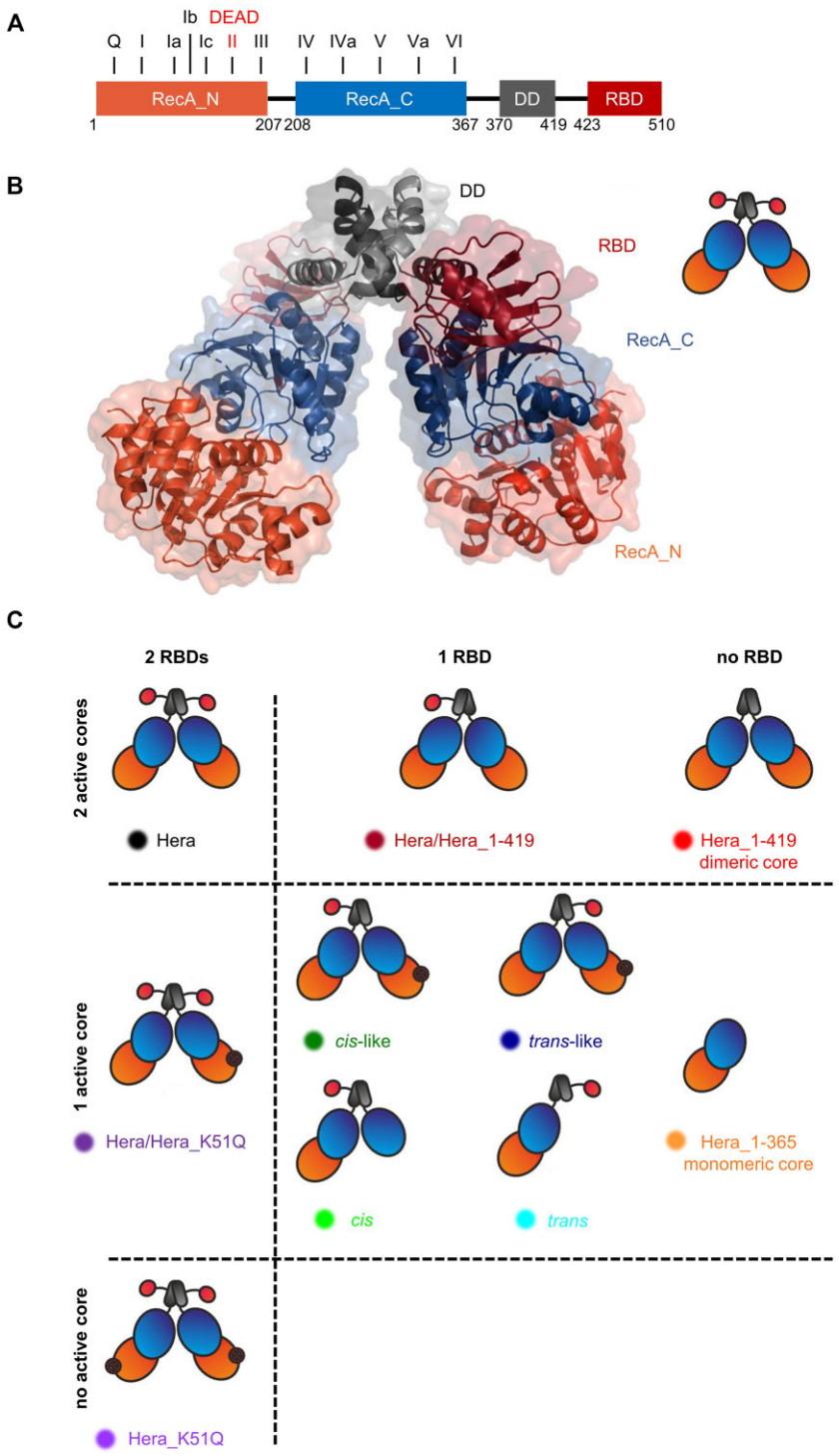

Figure 1. Architecture of Hera and constructs used in this study. (**A**) Domain architecture of Hera. The helicase core comprising the N-terminal and C-terminal RecA domains (RecA_N, RecA_C; orange, blue) carries the conserved motifs [Q, I, Ia, Ib, Ic, II (DEAD-box), and III in RecA_N, and IV, IVa, V, Va, and VI in RecA_C]. The C-terminal extension is formed by the DD (black) and the RBD (red). (**B**) Structural model of the Hera dimer [17, 19, 20]. The RecA_N and RecA_C of the helicase core are shown in orange and blue, the DD in black, and the RBD in red. The cartoon depiction used in the following is shown on the right. (**C**) Constructs used in this study and color code used throughout the manuscript for data sets obtained for these constructs. The color code for the domains is the same as in panels (A) and (B).

hairpins. In this binding mode, the central region of the RRM interacts with single-stranded RNA flanking the hairpin, and the C-terminal tail binds to the double-stranded stem [21].

In vivo, Hera binds to a large number of RNAs, consistent with a general role as an RNA chaperone [22]. *In vitro*, the RBD mediates binding of Hera to 23S rRNA fragments comprising hairpin 92 and to RNase P RNA [8]. Binding of these RNAs to Hera induces a conformational change of the helicase core to a compact, closed state [8, 22], leading to the formation of the catalytic site for ATP hydrolysis and the bipartite RNA binding site extending over both domains of the core [23]. Hera unwinds a minimal 32/9mer RNA substrate comprising hairpin 92 and an adjacent 9-bp helix derived from helix 91 of 23S rRNA in an ATP-dependent reaction *in vitro* [8]. The 32/9mer RNA substrate was originally identified as a minimal *in vitro* substrate for the DEAD-box protein DbpA (*Escherichia coli*) [24] and for its *Bacillus subtilis* homolog YxiN [11, 12, 25, 26], two helicases involved in ribosome biogenesis. This or similar hairpin-containing model substrates have also been used to characterize RNA binding and unwinding by CsdA and CshA [27, 28], helicases with the same domain architecture as Hera that also form stable dimers [27, 29]. CsdA and CshA have been associated with diverse functions, including ribosome biogenesis [30, 31], RNA decay, fatty acid homeostasis [32], quorum sensing [33], and cold adaptation [34–37].

In the Hera dimer, the active sites of the two helicase cores face toward each other, making a functional cooperation between the two cores possible. Such a cooperation may entail the interaction of both cores with the same RNA molecule or even the same duplex. However, the communication between the RBDs and the core within one protomer of the dimer, and between the RBDs and cores in different protomers is not understood. Here, we probe the role of the two RBDs by comparing the RNA-stimulated ATPase activities, RNA binding affinities and binding kinetics, RNA unwinding, and the RNA- and ATP-induced conformational change of the Hera helicase core in constructs containing both helicase cores, and two, one or no RBD(s). We then analyze the role of the two helicase cores, both in the presence and absence of the RBDs, by comparing Hera constructs containing two or no RBDs plus one or two (functional) cores. Finally, we probe the communication between RBDs and cores by comparing *cis*- and *trans*-(like) heterodimers with one (functional) helicase core and one RBD either on the same (*cis*, *cis*-like) or the other protomer (*trans*, *trans*-like). An overview about the different constructs used is shown in Fig. 1C. We show that the interaction of the RBD with the hairpin anchors Hera on the RNA, which then preferentially interacts with the helicase core on the same protomer. However, interactions with the other protomer are possible, especially in the presence of ATP. Hera with a single helicase core and an RBD on the same protomer has wildtype-like RNA-stimulated ATPase activity and RNA affinities, but its RNA helicase activity is reduced, suggesting different levels of cooperativity between the two protomers in ATP hydrolysis and RNA unwinding. The conformational change of the helicase core that is coupled to ATP hydrolysis and RNA unwinding is possible irrespective of the number of RBDs or cores, suggesting that an individual helicase core is a functional unwinding unit. Thus, domains outside the helicase core are not required for helicase activity under optimal conditions but ensure function at limiting conditions *in vivo*.

Materials and methods

Reagents

Reagents used in this study are detailed in Supplementary Table S1.

Biological resources

Biological resources used in this study are detailed in Supplementary Table S2.

Statistical analyses

Equations used to analyze data are detailed in the corresponding "Materials and methods" section. The number of replicate experiments (technical replicates) is indicated in the respective section as well as in the figure legends. Data from replicate ATPase assays, anisotropy titrations, and kinetic experiments on RNA binding and RNA unwinding were analyzed in concatenated fits of all data points obtained. Errors reported are the errors of these concatenated fits. Förster resonance energy transfer (FRET) efficiencies were extracted from individual FRET histograms, and mean values and the error of the mean was calculated from these individual values.

Novel programs, software, and algorithms

All software used in this work is commercially available or publicly available free of charge (see Supplementary Table S3).

Web sites/databases

This work used information from the PDB database. The web-based program Expasy [38] was used to calculate extinction coefficients of recombinant proteins (see Supplementary Table S3, S5).

Protein production and purification

All Hera constructs used in this study are summarized in Fig. 1C. Full-length Hera (Hera_1–510), Hera_1–419, and the ATPase-deficient variants Hera_1–510_K51Q and Hera_1–419_K51Q were produced with an N-terminal His_6-tag in *E. coli* Rosetta (DE3) cultivated in autoinducing medium [39] and purified on Ni^{2+}-NTA sepharose (Ni^{2+} sepharose 6 FF, 10 ml, equilibrated in 50 mM Tris–HCl pH 7.5, 500 mM NaCl, 20 mM imidazole; elution with 500 mM imidazole in the same buffer) and by size-exclusion chromatography (HiLoad 16/60 Superdex S200, equilibrated in 50 mM Tris–HCl pH 7.5, 500 mM NaCl). If necessary, an additional purification step on heparin sepharose (HiTrap Heparin HP, 10 ml) was performed (equilibration in 50 mM Tris–HCl pH 7.5, 100 mM NaCl; elution in the same buffer with 500–750 mM NaCl). Hera_1–365 (monomeric core) and Hera_208–419 (Hera_RecA_C_DD) were produced in *E. coli* Rosetta (DE3) in autoinducing medium [39] and purified as previously described [8, 19]. The His_6-GST-Hera_424–510 fusion protein (Hera_RBD) was purified on glutathione sepharose (GSTPrep FF 16/10, 20 ml), followed by size-exclusion chromatography (HiLoad 16/60 Superdex 75, GE Healthcare) [17, 18].

Cysteine variants (E115C/E227C), the ATPase-deficient K51Q variants, and the K463A variant were generated by site-directed mutagenesis [see Supplementary Table S4 for primer sequences, purchased desalted and dried from Sigma (Taufkirchen, Germany)] and purified according to the protocols described above, except that 2 mM β-mercapto ethanol

(β-ME) was added to all buffers for constructs containing cysteines.

For the preparation of heterodimers, His_6-Hera_1–419, His_6-Hera_1–419_K51Q, or His_6-Hera_1–510_K51Q containing a thrombin cleavage site following the His_6-tag were cleaved by thrombin after the first Ni^{2+}-NTA purification step; uncleaved fusion protein was removed by a second Ni^{2+}-NTA purification step. Heterodimers were generated by mixing a 5-fold molar excess of the variant without tag with the His_6-tagged variant, followed by incubation at 65°C for 1 h to accelerate subunit exchange [19]. The resulting heterodimers were purified by Ni^{2+}-NTA sepharose and size-exclusion chromatography as described above.

All Hera constructs containing the DD eluted as dimers from the size-exclusion column. Protein concentrations were determined photometrically by measuring the absorption at 280 nm. Extinction coefficients were calculated for dimers from the sequence of the two protomers with Expasy ProtParam [38] (Supplementary Table S5).

RNA substrates

RNA oligonucleotides were purchased PAGE-purified from Sigma; fluorescently labeled RNAs were high-performance liquid chromatography (HPLC)-purified. The sequences were: 5′-GCAGGUCCCAAGGGUUGGGCUGUUCGCCCAUU-3′ (32mer), 5′-UUGGGACCU-3′ (9mer), and 5′-AGGUCCCAA-3′ (9mer_comp). The regions of the 32mer forming the stem of hairpin 92 are underlined. Fl-32mer and Cy5-32mer are identical in sequence to the 32mer but contain a fluorescein/Cy5 modification attached to the 5′-end. 9mer-Cy3 is identical to the 9mer but carries a Cy3 modification at the 3′-end.

ATPase activity

Steady-state ATPase activity was measured in a coupled enzymatic assay that couples the hydrolysis of ATP to NADH oxidation. Measurements were performed at 37°C with 0.15 μM Hera or Hera_1–419 (0.3 μM for all heterodimers and Hera_1–365) in 50 mM Tris–HCl, pH 7.5, 150 mM NaCl, and 5 mM $MgCl_2$ in the presence of 1.6 mM NADH, 0.8 mM phosphoenol pyruvate, 92 $\mu g \cdot ml^{-1}$ pyruvate kinase, and 52 $\mu g \cdot ml^{-1}$ lactate dehydrogenase as described [8]. Poly-U RNA was added at different concentrations from 0 to 1000 μM bases. Reactions were started by addition of 5 mM ATP. Reaction velocities v of ATP hydrolysis were obtained from the change in absorption with time:

$$v = \frac{\Delta A_{340}}{\Delta t \cdot d \cdot \varepsilon_{340,\,\mathrm{NADH}}} \tag{1}$$

where ΔA_{340} is the change in absorption, Δt is the observed time interval, d is the pathlength (1 cm), and $\varepsilon_{340,\,\mathrm{NADH}}$ is the molar extinction coefficient of NADH at 340 nm [40]. The dependence of the reaction velocity on RNA concentration $c_{\text{poly-U}}$ was described with a modified Michaelis–Menten equation:

$$v = v_0 + \frac{v_{\max} \cdot c_{\text{poly}-U}}{K_{1/2,\mathrm{RNA}} + c_{\text{poly}-U}} \tag{2}$$

v_0 is the intrinsic ATP hydrolysis rate in the absence of RNA, $v_{\max}$ is the maximum increase in velocity at saturating RNA concentrations, and $K_{1/2,\mathrm{RNA}}$ is the RNA concentration at which RNA-stimulated ATPase activity occurs with half-maximum velocity. The catalytic turnover number k_{cat} was calculated by the division of $v_{\max}$ by the enzyme concentration, and the catalytic efficiency is determined as the ratio of k_{cat} and $K_{1/2,\mathrm{RNA}}$. Errors σ for the catalytic efficiency were calculated from the errors of k_{cat} and $K_{1/2,\mathrm{RNA}}$ according to the propagation of uncertainties with the following equation:

$$\sigma\left(\frac{k_{\mathrm{cat}}}{K_{1/2,\mathrm{RNA}}}\right) = \sqrt{\sigma_{k_{\mathrm{cat}}}^2 \cdot \left(\frac{1}{K_{1/2,\mathrm{RNA}}}\right)^2 + \sigma_{K_{\mathrm{M}}}^2 \cdot \left(-\frac{k_{\mathrm{cat}}}{K_{1/2,\mathrm{RNA}}}\right)^2} \tag{3}$$

Values for k_{cat} and $K_{1/2,\mathrm{RNA}}$ are summarized in Table 1.

Determination of K_d values in fluorescence equilibrium titrations

K_d values for Hera/RNA complexes were determined in fluorescence anisotropy titrations of 0.05 μM 32mer or fl-32/9mer (fl-32mer with the 9mer annealed) in 50 mM Tris–HCl, pH 7.5, 150 mM NaCl, and 5 mM $MgCl_2$ with Hera and Hera variants as described [8] using a Jobin Yvon FluoroMax3 fluorimeter. Fluorescence was excited at 496 nm (2 nm bandwidth) and detected at 520 nm (4 nm bandwidth). Data were analyzed using the solution of the quadratic equation that describes a 1:1 complex formation:

$$r = r_0 + \Delta r_{\max} \cdot f_{\mathrm{bound}} \tag{4}$$

where r_0 is the anisotropy of free RNA, $\Delta r_{\max}$ is the amplitude ($r_{\mathrm{bound}} - r_{\mathrm{free}}$), and f_{bound} is

$$f_{\mathrm{bound}} = \frac{\frac{[Hera]_{\mathrm{tot}}+[RNA]_{\mathrm{tot}}+K_d}{2} - \sqrt{\left(\frac{[Hera]_{\mathrm{tot}}+[RNA]_{\mathrm{tot}}+K_d}{2}\right)^2 - [Hera]_{\mathrm{tot}}[RNA]_{\mathrm{tot}}}}{[RNA]_{\mathrm{tot}}} \tag{5}$$

with the total Hera (dimer) concentration $[Hera]_{\mathrm{tot}}$, the total RNA concentration $[RNA]_{\mathrm{tot}}$, and the dissociation constant K_d. K_d values for Hera/RNA complexes determined with Equation (4) are summarized in Table 2. To determine accurate K_d values from anisotropy titrations, changes in fluorescence intensity F on binding, $R = F_{\mathrm{bound}}/F_{\mathrm{free}}$, need to be taken into account. However, both analyses gave similar values for all constructs (Supplementary Table S6), and the relative K_d values for the constructs compared within each set of comparisons are unaffected by the value of R used in the analysis in all cases.

Alternatively, K_d values were determined using numerical analyses based on explicit models using Dynafit [41, 42] (see Supplementary data for Dynafit scripts). In the simplest case, binding of RNA to Hera dimers was described as independent, single-step binding to each protomer, with K_d values and the anisotropy of free (r_{free}) and bound RNA (r_{bound}) as fit parameters. These values are summarized in Table 2. For heterodimers, K_{d1} and K_{d2} were used to describe the interaction of the RNA with the two different protomers. As kinetic experiments on RNA binding suggested two-step binding of RNA to Hera, models describing RNA binding in two steps, with parameters K_{d1}, k_2 and k_{-2}, r_{free} and r_{bound}, were also used. The models used are provided in the respective figures alongside with the experimental data and fits.

Stopped-flow experiments

Binding of the fl-32mer or the fl-32/9mer was measured in a TgK KinetAsyst SF-61DX2 Stopped-flow system, using the

fluorescence intensity of the fl-32mer as a probe for binding. The fl-32mer (0.05 μM) in 50 mM Tris–HCl, pH 7.5, 150 mM NaCl, and 5 mM $MgCl_2$ in the observation chamber was used as a reference signal. The intensities for the parallel and perpendicular orientation of the polarizers were adjusted by changing the voltage of the photomultiplier such that the *G*-factor had a value of one. Fl-32mer was excited with an LED L470A (Ocean Optics, Ostfildern, Germany), and emitted light was detected through a cut-off filter of 515 nm in photomultiplier. Stopped-flow traces were measured over 0.5 s (2048 data points) at 25°C after 1:1 mixing of the fl-32mer with Hera. The observed rate constants k_{obs} were determined by describing the traces with single-exponential functions. From the hyperbolic dependence of k_{obs} on Hera concentration, the parameters for two-step binding were extracted according to the following equation:

$$k_{obs} = k_{-2} + k_2 \cdot \frac{[Hera]}{K_{d1} + [Hera]} \quad (6)$$

K_{d1} is the dissociation constant of the initial Hera/RNA complex, [*Hera*] is the concentration of Hera, k_2 and k_{-2} are the rate constants of the forward and reverse reactions of a second step following the formation of the initial complex, and their ratio k_{-2}/k_2 defines K_{d2}. The errors of k_2 and k_{-2} were propagated to K_{d2} according to the following equation:

$$\sigma\,(K_{d2}) = \sqrt{\sigma_{k_{-2}}^2 \cdot \left(\frac{1}{k_2}\right)^2 + \sigma_{k_2}^2 \cdot \left(-\frac{k_{-2}}{(k_2)^2}\right)^2} \quad (7)$$

The overall K_d can be calculated from K_{d1}, k_2, and k_{-2} as:

$$K_d = K_{d1} \cdot \frac{k_{-2}}{k_2} = K_{d1} \cdot K_{d2} \quad (8)$$

The errors from K_{d1} and K_{d2} were propagated to K_d as:

$$\sigma\,(K_d) = \sqrt{\sigma_{K_{d1}}^2 \cdot (K_{d2})^2 + \sigma_{K_{d2}}^2 \cdot (K_{d1})^2} \quad (9)$$

In few cases, k_{obs} showed a linear dependence on Hera concentration, characteristic for one-step binding. In these cases, the rate constants k_1 and k_{-1} for binding and dissociation were obtained from the slope and *y*-axis intercept according to the following equation:

$$k_{obs} = k_{-1} + k_1 \cdot [Hera] \quad (10)$$

Error propagation to $K_d = k_{-1}/k_1$ was done in analogy to equation (3). Rate constants and equilibrium constants determined from the concentration dependence of k_{obs} are summarized in Table 3.

RNA unwinding

RNA unwinding was followed as a function of time using a Cy3/Cy5-labeled 32/9mer unwinding substrate and measuring the decrease in FRET upon unwinding as a spectroscopic probe. The substrate for unwinding was generated by incubating a 2-fold molar excess of the 3′-Cy3-labeled 9mer with the 5′-Cy5-labeled 32mer in 50 mM Tris–HCl, pH 7.5, 150 mM NaCl, and 5 mM $MgCl_2$ at 95°C for 5 min and slowly cooled to 25°C. Unwinding reactions were performed in 50 mM Tris–HCl, pH 7.5, 150 mM NaCl, and 5 mM $MgCl_2$ at 25°C with 0.5 μM RNA substrate and 0.25–7.5 μM Hera in the presence of 5 μM unlabeled 9mer_comp RNA as a trap to prevent reannealing. Reactions were started by the addition of 5 mM ATP. The donor (Cy3) was excited at 554 nm (1 nm bandwidth), and unwinding was followed as a decrease in acceptor (Cy5) emission at 666 nm (2 nm bandwidth). A rate constant k_{obs} was obtained from describing the data with a single-exponential function. The dependence of the observed rate constant on the concentration of Hera was described by a hyperbola to determine the unwinding rate constant (turnover number), k_{unw}, and the corresponding equilibrium constant, $K_{1/2,unw}$:

$$k_{obs} = k_{unw} \cdot \left(\frac{[Hera]}{K_{unw} + [Hera]}\right) \quad (11)$$

$K_{1/2,unw}$ is the concentration of Hera at which the unwinding rate is half-maximal. Values for k_{unw} and $K_{1/2,unw}$ are summarized in Table 4.

Single-molecule FRET experiments

Single-molecule FRET experiments were performed on a Microtime 200 confocal fluorescence microscope (PicoQuant). Cuvettes were pre-incubated for 30 min with 10 μM of the ATPase-deficient Hera_K51Q variant in activity buffer. Labeling of Hera_E115C/E227C (50–100 μM) was performed in 50 mM Tris–HCl, pH 7.5, 750 mM NaCl, and 1 mM tris(2-carboxyethyl)phosphine with a 3-fold molar excess of AlexaFluor 488 (donor) and 6-fold molar excess of AlexaFluor 546 (acceptor) for 1 h at 25°C. Free dye was removed by size-exclusion chromatography (Micro BioSpin P30, Bio-Rad). Donor fluorescence was excited with the output from a pulsed LDH-PFA-488 laser diode (40 MHz), focused by a 60× water immersion objective (UPlanAPO NA 1.2, Olympus, München, Germany). Fluorescence emission was separated from excitation light by a beam splitter (500 dcr), further split into donor and acceptor emission with a dichroic mirror (Z532 rdc), passed through 535/40 (donor) and 570/LP (acceptor) filters, and detected via τ-single-photon avalanche diode (τ-SPAD) detectors (PicoQuant, Berlin, Germany). Measurements were performed with 200 pM of labeled protein (donor concentration) in 50 mM Tris–HCl, pH 7.5, 150 mM NaCl, and 5 mM $MgCl_2$ at 25°C for 30 min either in the absence or presence of 0.8–4.8 μM 32mer and 5 mM 5'-adenylyl-β,γ-imidotriphosphate (ADPNP) to induce conformational changes. FRET histograms were constructed from FRET efficiencies calculated from fluorescence bursts of >80 photons using SymPhoTime 64 v2.4.4874 (PicoQuant, Berlin, Germany). Cross-talk between donor and acceptor channels and differences in detection efficiencies and quantum yields were removed by applying correction parameters ($\alpha' = 0.445$, $\beta' = 0$, and $\gamma' = 1.401$; see [43]). FRET histograms were analyzed in OriginPro 2023 (OriginLab, Northampton, USA).

Results

Role of the RBDs: Hera containing two, one, or no RBDs

To dissect the role of the two RBDs for RNA unwinding by Hera, we generated a heterodimer with only a single RBD, containing one copy of full-length Hera and one copy of Hera_1–419 lacking the RBD (Hera/Hera_1–419; Fig. 1C). We then compared its RNA-stimulated ATPase activity, RNA binding, and unwinding properties (Fig. 2) as well as its conformational response to RNA and ADPNP (Fig. 3) with Hera (containing two RBDs) and with the dimeric core without RBDs (Hera_1–419) .

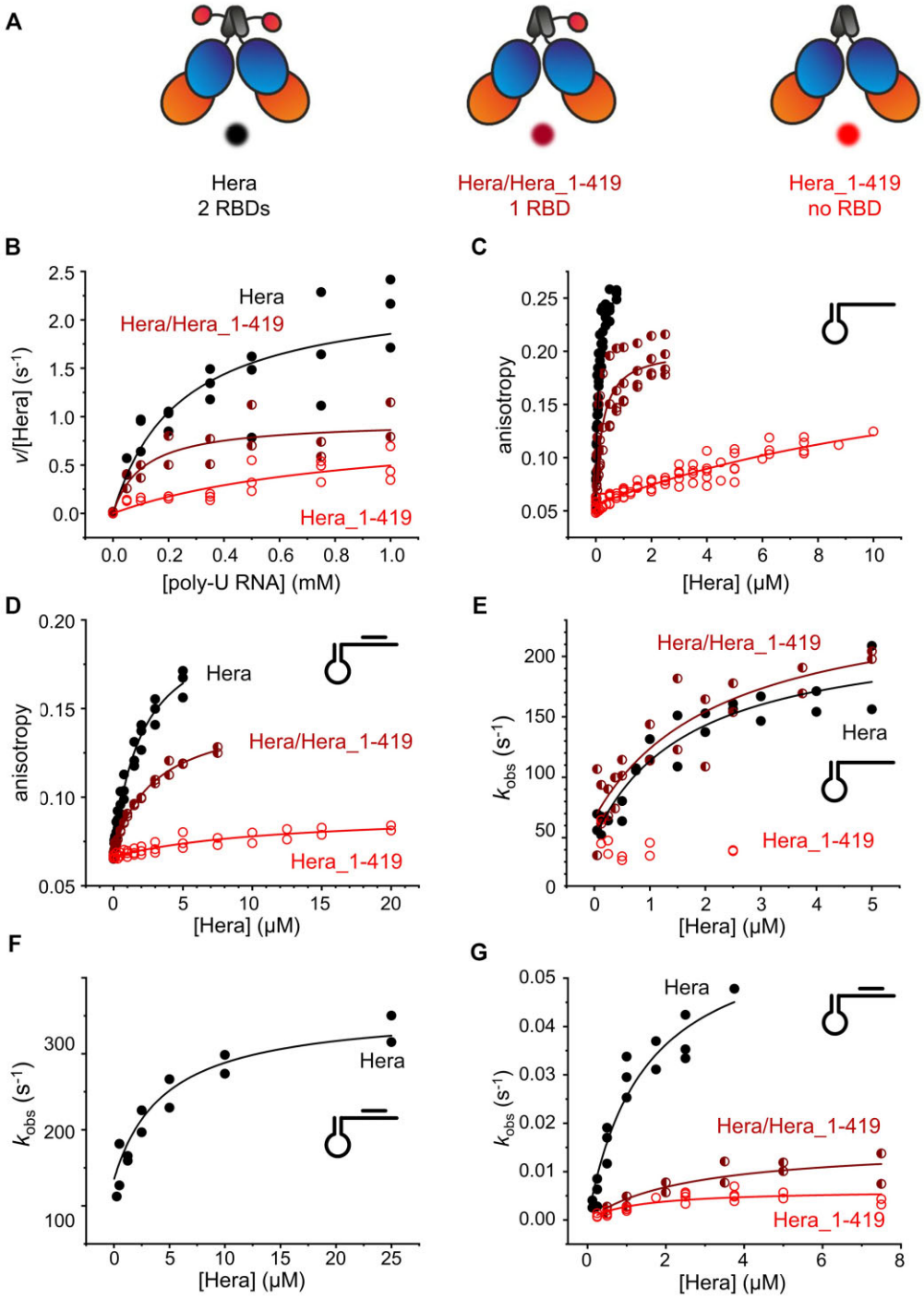

Figure 2. Effect of the RBDs on RNA-stimulated ATPase activity, RNA binding, and unwinding. (**A**) Hera constructs with two cores and two, one, and no RBD. Hera (two cores, two RBDs; black, filled circles), Hera/Hera1-419 (heterodimer, two cores, one RBD; brown, half-filled circles), and Hera_1–419 (dimeric core: two cores, no RBD; red, open circles). (**B**) RNA-dependent ATPase activity of 0.15 μM of Hera (two RBDs; black, filled circles), 0.30 μM of Hera/Hera_1–419 (one RBD; brown, half-filled circles), and 0.15 μM of Hera_1–419 (no RBD; red, open circles). Data are cumulative data points from at least two independent experiments. The lines are cumulative fits to all data points with the Michaelis–Menten equation (see "Materials and methods" section). Original data are shown in Supplementary Fig. S1A. (**C**) Fluorescence equilibrium titrations of single-stranded 32mer RNA with Hera (black, filled circles), Hera/Hera_1–419 (brown, half-filled circles), and Hera_1–419 (red, open circles). Lines are fits according to a 1:1 binding model (see "Materials and methods" section). Hera concentrations are given as concentrations of dimer. (**D**) Fluorescence equilibrium titrations of double-stranded 32/9mer RNA with Hera (black, filled circles). Lines are fits according to a 1:1 binding model (see "Materials and methods" section). Hera concentrations are given as concentrations of dimer. (**E**) Concentration dependence of observed rate constants k_{obs} for binding of Hera (black, filled circles), Hera/Hera_1–419 (brown, half-filled circles), and Hera_1–419 (red, open circles) to 32mer RNA. Rate constants were obtained by describing stopped-flow traces (see Supplementary Fig. S1B) with single-exponential functions. (**F**) Concentration dependence of observed rate constants k_{obs} for binding of Hera (black, filled circles) to 32/9mer RNA. Rate constants were obtained by describing stopped-flow traces with single-exponential functions. (**G**) Concentration dependence of observed rate constants k_{obs} for 32/9mer unwinding by Hera (black, filled circles), Hera/Hera_1–419 (brown, half-filled circles), and Hera_1–419 (red, open circles). Rate constants were obtained by describing the fluorescence traces (see Supplementary Fig. S1C) with single-exponential functions.

RNA-stimulated ATPase activity

The RNA-stimulated ATPase activity was measured in a steady-state ATPase assay as a function of the concentration of poly-U RNA (Fig. 2B, Supplementary Fig. S1A, and Table 1). poly-U RNA is a mixture of single-stranded RNAs of different lengths (see Supplementary Table S1): it interacts with and activates the ATPase activity of the helicase core of Hera [8]. Uridine can only be accommodated at positions 3 and 4 of the four positions forming the RNA recognition site on the RBD [21], enabling no or only weak interactions of poly-U with the RBD.

Hera, Hera/Hera_1–419, and Hera_1–419 showed a hyperbolic dependence of the reaction velocity for ATP hydrolysis on the concentration of poly-U (Fig. 2B). The k_{cat} value at saturating RNA concentrations was $k_{cat} = 2.3 \pm 0.3\ s^{-1}$ for Hera (two RBDs). For Hera/Hera_1–419 and Hera_1–419, the values were lower ($k_{cat} = 1.0 \pm 0.1\ s^{-1}$ for Hera/Hera_1–419, one RBD, and $k_{cat} = 0.9 \pm 0.3\ s^{-1}$ for Hera_1–419, no RBDs; Table 1). Note that the protein concentrations are given in terms of (hetero-)dimers; hence, these k_{cat} values reflect the turnover by both cores. The turnover numbers per core would be half of these values. However, as these constructs contain the same number of cores, the turnover numbers can be compared directly. The lower k_{cat} of Hera lacking one or both RBDs compared to the k_{cat} of Hera with both RBDs points to a role of the RBDs for RNA-stimulated ATP hydrolysis, even with poly-U RNA that predominantly interacts directly with the core. The $K_{1/2,RNA}$ values were 240 ± 84 μM (nucleotides) for Hera, 108 ± 51 μM for Hera/Hera_1–419, and 871 ± 552 μM for Hera_1–419 (Table 1). These values reflect the $K_{1/2}$ for the RNA binding site in the helicase core. Although a conclusion on the effect of deleting the RBDs is limited by the large error of the $K_{1/2,RNA}$ value for Hera_1–419, the data are suggestive of a role of the RBDs in the stimulation of the ATPase activity by poly-U RNA, both on the level of binding ($K_{1/2}$) and catalysis (k_{cat}).

The catalytic efficiency, $k_{cat}/K_{1/2,RNA}$, is identical for Hera (two RBDs) and Hera/Hera_1–419 (one RBD), with values of $k_{cat}/K_{1/2,RNA} = 0.009 \pm 0.002\ \mu M^{-1}\ s^{-1}$ (Hera) or $0.009 \pm 0.003\ \mu M^{-1}\ s^{-1}$ (Hera/Hera_1–419). For Hera_1–419 (no RBDs), the catalytic efficiency was reduced 9-fold, to $0.001 \pm 0.0007\ \mu M^{-1}\ s^{-1}$. Thus, deleting one RBD does not have much of an effect, but deleting the second RBD substantially reduces the catalytic efficiency of RNA-stimulated ATP hydrolysis.

Overall, the intrinsic ATPase activity of Hera is also stimulated in the presence of poly-U RNA in the absence of the RBDs, in agreement with direct binding of poly-U RNA to the two helicase cores present in all three constructs. While deletion of one or both RBDs leads to a decrease in k_{cat}, $K_{1/2,RNA}$ increases only when both RBDs are deleted. This behavior points to some interaction of poly-U with the RBDs and suggests some contributions of the RBDs to RNA-stimulated ATP hydrolysis by the cores.

RNA affinity: anisotropy titrations

Next, we analyzed the effect of the number of RBDs on RNA binding in fluorescence anisotropy titrations of a fluorescein-labeled 32mer and 32/9mer with Hera, Hera/Hera_1–419, and Hera_1–419 (Fig. 2C and D, and Table 2). These RNAs contain a hairpin that binds to the RBD, and a flanking single- or double-stranded region that interacts with the helicase core [21]. The titration curves of these RNAs with Hera, Hera/Hera_1–419, and Hera_1–419 were hyperbolic, with no indication of sigmoidality, suggesting that binding of the RNA to the Hera dimer is non-cooperative. Consistent with this, all titration curves could be described by a 1:1 binding model (Equations 4 and 5). For the Hera/32mer complex, a K_d value of 0.06 ± 0.01 μM was obtained. For the 32/9mer complex, the K_d value was 33-fold higher, with $K_d = 2.0 \pm 0.3$ μM. For Hera/Hera_1–419 (one RBD), slightly higher dissociation constants were obtained, with K_d values of 0.25 ± 0.09 μM (32mer) and 3.0 ± 0.3 μM (32/9mer; 12-fold higher than 32mer). Hera_1–419 (no RBD) showed the highest dissociation constants, with a K_d of 16 ± 7 μM (32mer) and 11 ± 5 μM (32/9mer).

Note that the K_d values determined in anisotropy titrations need to be interpreted with care because of the dimeric nature of the Hera constructs, and also because the 32/9mer can interact with different regions of Hera: for Hera_1–419, lacking RBDs, the RNA must interact with the cores, and the concentration of cores is twice the dimer concentration. In this case, the K_d values for each core of the dimer are thus twice the values determined, i.e. 32 μM (32mer) and 22 μM (32/9mer). The (isolated) helicase core of Hera thus has a slight, if any, preference for double-stranded over single-stranded RNA.

In contrast to Hera_1–419, the K_d values for the Hera/32mer and the Hera/32/9mer complexes reflect both the interaction of the RBDs with the hairpin [21] and the interaction of the flanking single- or double-stranded region with the helicase core. The apparent K_d values of $K_d = 0.06 \pm 0.01$ μM (32mer) and $K_d = 2.0 \pm 0.3$ μM (32/9mer) correspond to $K_d = 0.12$ μM per protomer (32mer, in excellent agreement with the previously reported value of 0.13 μM [21]) and $K_d = 4.0$ μM (32/9mer). With the assumption that the interactions of Hera with the hairpin and the flanking single- or double-stranded region are independent and represented by K_{d1} (interaction with the RBDs) and $K_{d2,ss}$ or $K_{d2,ds}$ (interaction of the flanking single- or double-stranded RNA with the cores; see schematic in Supplementary Fig. S2A,B), the overall K_d measured must correspond to the product of K_{d1} and either $K_{d2,ss}$ (32mer) or $K_{d2,ds}$ (32/9mer). The ratio of the overall K_d values for 32mer and 32/9mer then directly reflects the ratio $K_{d2,ds}/K_{d2,ss} = 33$, meaning the Hera core interacts 33-fold more strongly with single-stranded than with double-stranded RNA when the hairpin is pre-bound (note that $K_{d2,ss}$ or $K_{d2,ds}$ reflect the K_d values for a unimolecular interaction, not for the bimolecular interaction of the Hera core with single- or double-stranded RNA. The corresponding value for the bimolecular interaction, obtained from the comparison of the corresponding K_d values for the Hera_1–419 complexes, suggest little preference, see Table 2). Thus, the core only shows a preference for single-stranded RNA when the RNA is anchored to the RBD.

Finally, the K_d values for Hera/Hera_1–419 (two cores, one RBD) can be rationalized by binding of the hairpin to the one RBD in the Hera protomer, followed by an interaction of the flanking region with the core in this protomer (with an overall K_d of K_{d1} multiplied with $K_{d2,ss}$ or $K_{d2,ds}$, where K_{d2} again represents the unimolecular rearrangement) and by the direct binding of the single- or double-stranded region of a second RNA molecule to the core in the Hera_1–419 protomer ($K_{d,core,ss}$ or $K_{d,core,ds}$, reflecting the bimolecular association of the RNA with the core; see Supplementary Fig. S2C). The K_d values of 0.25 and 3.0 μM retrieved by analysis of the titra-

Table 1. ATPase activity

	RBDs	(functional) cores	k_{cat} (s^{-1})	k_{cat} (s^{-1}) per (functional) core[a]	$K_{1/2,RNA}$ (μM)
# of RBDs					
Hera	2	2	2.3 ± 0.3	1.2 ± 0.1	240 ± 84
Hera/Hera_1–419	1	2	1.0 ± 0.1	0.48 ± 0.06	108 ± 51
Hera_1–419	0	2	0.9 ± 0.3	0.5 ± 0.2	871 ± 552
# of (functional) cores					
Hera	2	2	2.3 ± 0.3	1.2 ± 0.1	240 ± 84
Hera/Hera_K51Q	2	1	1.19 ± 0.05	1.19 ± 0.05	109 ± 18
Hera_K51Q	2	0	n.a[b]	n.a.	n.a.
Hera_1–419	0	2	0.9 ± 0.3	0.5 ± 0.2	871 ± 552
Hera_1–365	0	1	n.d.[c]	n.d.	n.d.
position of RBD					
Hera	2	2	2.3 ± 0.3	1.2 ± 0.1	240 ± 84
cis	1	1	1.2 ± 0.1	1.2 ± 0.1	200 ± 52
trans	1	1	1.9 ± 0.4	1.9 ± 0.4	697 ± 227
cis-like	1	1	0.3 ± 0.09	0.3 ± 0.09	519 ± 357
trans-like	1	1	0.7 ± 0.2	0.7 ± 0.2	1113 ± 486

[a]Concentrations of Hera are given as dimer concentrations. The k_{cat} values per (functional) core is obtained by dividing the k_{cat} value by the number of (functional) cores present. $K_{1/2,app,RNA}$ does not depend on the Hera concentration, which is limiting in these experiments, and directly reflects the apparent affinity of the Hera core for poly-U RNA.
[b]n.a.: not applicable.
[c]n.d.: not detected.
Errors are the errors of the concatenated fit of the cumulative data from at least two independent experiments.

Table 2. RNA affinities

	RBDs	cores	K_d (μM) (32mer)	K_d (μM) (32/9mer)	K_d (μM) (32mer) per protomer[a]	K_d (μM) (32/9mer) per protomer[a]
# of RBDs						
Hera	2	2	0.06 ± 0.01	2.0 ± 0.3	0.11 ± 0.02	4.0 ± 0.6
					0.13 ± 0.02	4.1 ± 0.63
Hera/Hera_1–419	1	2	0.25 ± 0.09	3.0 ± 0.3	0.50 ± 0.18	6.0 ± 0.6
					0.5 ± 0.18	6.0 ± 0.6
Hera_1–419	0	2	16 ± 7	11 ± 5	32 ± 14	22 ± 10
					34 ± 15	23 ± 11
# of (functional) cores						
Hera	2	2	0.06 ± 0.01	2.0 ± 0.3	0.11 ± 0.02	4.0 ± 0.6
					0.13 ± 0.02	4.1 ± 0.63
Hera/Hera_K51Q	2	1	0.08 ± 0.02	2.5 ± 0.4	0.16 ± 0.04	5.0 ± 0.8
					0.20 ± 0.072	5.0 ± 0.82
Hera_K51Q	2	0	0.17 ± 0.02	2.1 ± 0.4	0.34 ± 0.04	4.2 ± 0.8
					0.36 ± 0.042	4.3 ± 0.84
Hera_1–419	0	2	16 ± 7	11 ± 5	32 ± 14	22 ± 10
					34 ± 15	23 ± 11
Hera_1–365	0	1	81 ± 29	n.d.[b]	81 ± 29	n.d.
position of RBD						
Hera	2	2	0.06 ± 0.01	2.0 ± 0.3	0.11 ± 0.02	4.0 ± 0.6
					0.13 ± 0.02	4.1 ± 0.63
cis	1	1	0.126 ± 0.009	1.4 ± 0.5	0.126 ± 0.009	1.4 ± 0.5
trans	1	1	3.1 ± 0.5	16 ± 6	3.1 ± 0.5	16 ± 6
cis-like	1	1	n.d.	n.d.	n.d.	n.d.
trans-like	1	1	n.d.	n.d.	n.d.	n.d.
RBD	1	0	1.0 ± 0.2	17 ± 3	1.0 ± 0.2	17 ± 3

Values were determined from analyses of anisotropy titrations using equation (4) (upper row) or from numerical analyses with Dynafit (bottom row, see text).
[a]As Hera concentrations are given as dimer concentrations, the K_d values determined here reflect the values for both protomers. For homodimers, the true K_d value per protomer is obtained by multiplying K_d by two; for heterodimers, formed by protomers with different RNA affinities, multiplying the value by two gives an apparent K_d value per protomer.
[b]n.d.: not determined
Errors are the errors of the concatenated fit of the cumulative data from at least two independent experiments.

tion of Hera/Hera_1–419 with Equation (4) are between the values determined for Hera and Hera_1–419 (Table 2), suggesting that they represent apparent K_d values for binding of the RNA to the two protomers with different affinities.

Notably, the changes in anisotropy (final values) are markedly different for the different Hera variants and for the binding of single-stranded versus double-stranded RNAs (Fig. 2C and D). While RNA bound to Hera reaches an anisotropy of ∼0.3 (∼0.18 for the 32/9mer), this value is reduced to ∼0.2 (∼0.14 for 32/9mer) for Hera/Hera_1–419, and even more so, to ∼0.1 (∼0.08 for 32/9mer) for Hera_1–419. These differences are larger than expected from the only moderate differences of these variants in molecular mass (115, 104, and 96 kDa, respectively), pointing to different mobilities of the fluorophore in the different complexes, and different modes of binding. Interaction of the RNAs with the RBD (in Hera and in one protomer of Hera/Hera_1–419) is associated with a higher anisotropy increase, interaction with the core (in Hera_1–419) with a lower increase. Again, the values for the Hera/Hera_1–419 heterodimer are in-between the values for Hera and Hera_1–419, consistent with a preferential interaction of the RNA with the RBD of the Hera protomer, and an interaction with the core in the Hera_1–419 protomer. The different anisotropy values of 32mer and 32/9mer bound to Hera further suggest that these RNAs are bound differently. The higher anisotropy of the bound 32mer is consistent with its predominant interaction with the RBDs, whereas the lower anisotropy of the bound 32/9mer may suggest more contributions of the cores to the interaction.

Overall, the anisotropy titrations show that Hera interacts more strongly with hairpins flanked by single-stranded region than with the hairpin flanked by a duplex. Removal of one or both RBDs reduces the overall RNA affinity of Hera. Notably, removal of the second RBD has a larger effect (64-fold/4-fold reduction in affinity for single- and double-stranded RNA, respectively) than removal of the first RBD (4-fold/1.5-fold). The decrease in RNA affinity is more pronounced for single- than for double-stranded RNA, which reduces the discrimination between single- and double-stranded RNA from 33-fold (two RBDs) to 12-fold (one RBD) and to no preference (no RBD; see Table 2).

RNA affinity: a quantitative model for RNA binding

To derive a quantitative model for RNA binding to Hera (see Supplementary Fig. S2), we performed numerical analyses of the titration data with one-step binding models for each protomer using Dynafit (see Supplementary data for Dynafit scripts). First, we validated this approach with the Hera and Hera_1–419 homodimers. The K_d values from the numerical analyses are in excellent agreement with the values determined from analyses using the Equation (4) (see Table 2; Supplementary Fig. S3A and B, see Supplementary data for a more detailed description of Dynafit analyses).

For the Hera/Hera_1–419 heterodimer, we also obtained values in excellent agreement with the value from the analysis using Equation (4). However, this analysis does not account for the different RNA affinities of the two protomers. A simulated titration curve based on a model that assumes independent binding of the 32mer to the Hera or Hera_1–419 protomers, using the parameter values determined from the Hera and Hera_1–419 titrations either with Dynafit, or with Equation (4) (Supplementary Fig. S3C; see Dynafit Script 2), roughly reflect the overall shape of the experimental binding curve, but does not describe the amplitude of the titration data satisfactorily. When we attempted to vary the K_d values for the binding events in the two protomers during a fit, they were highly correlated and could not be determined independently from the fit, precluding further quantitative analysis.

We performed the same analyses for the titrations of the 32/9mer with Hera/Hera_1–419 (Supplementary Fig. S3C; see Dynafit Script 1). Again, we reached excellent agreement with the results from the analysis with Equation (4). Simulations of binding curves with independent binding of the 32/9mer to the Hera or Hera_1–419 protomers with different affinities (see Dynafit Script 2) gave reasonable descriptions of the experimental data (Supplementary Fig. S3C).

Collectively, our binding data show that Hera and Hera_1–419 interact differently with the 32mer and the 32/9mer. Although we cannot derive a complete quantitative model for RNA binding by Hera/Hera_1–419 based on the simple analysis of the set of anisotropy titrations performed here, RNA binding to the two protomers in Hera/Hera_1–419 is consistent with the parameters for RNA binding to the individual protomers.

RNA binding kinetics

To further investigate the differences in interactions with RNA of Hera with two, one, or no RBD(s), we determined rate constants for RNA binding for all three constructs. To this end, we performed stopped-flow experiments and mixed a constant concentration of fl-32mer with increasing concentrations of Hera, Hera/Hera_1–419, or Hera_1–419. As we did not manage to obtain binding transients with sufficient signal-to-noise ratio using anisotropy as a signal, we followed complex formation as an increase in fluorescence intensity. All three variants caused a rapid increase in fluorescence within <0.1 s that could be described by a single-exponential function (Supplementary Fig. S1B). The observed rate constants k_{obs} determined from single-exponential fits showed a hyperbolic dependence on Hera concentration (Fig. 2E), in agreement with a two-step binding process, consisting of a first, spectroscopically silent binding step, followed by a slower, second step associated with a change in signal. Using Equation (6), K_{d1} for formation of the initial complex, as well as the rate constants k_2 and k_{-2} for the subsequent rearrangement of the collision complex were determined from the concentration dependence of k_{obs}. For Hera, we obtained values of $K_{d1} = 1.7 \pm 0.7$ μM, $k_2 = 173 \pm 21$ s^{-1}, and $k_{-2} = 50 \pm 9$ s^{-1}, which gives $K_{d2} = 0.29 \pm 0.06$ and $K_d = 0.49 \pm 0.22$ μM (Table 3 (a); note that K_{d1} again reflects the initial interaction of RNA with the dimer. K_{d1} and hence also K_d need to be doubled to calculate the value per protomer). The corresponding values for Hera/Hera_1–419 (one RBD) were $K_{d1} = 2.3 \pm 1.5$ μM, $k_2 = 188 \pm 44$ s^{-1} and $k_{-2} = 66 \pm 11$ s^{-1}, giving $K_{d2} = 0.35 \pm 0.10$ and $K_d = 0.81 \pm 0.64$ μM. For Hera_1–419 (no RBD), the observed rate constants showed no clear dependence on the concentration of Hera in the concentration range tested (up to 5 μM), consistent with little binding due to the lower 32mer affinity observed in equilibrium titrations ($K_d = 16$ μM, see Table 2).

Two-step binding of RNA to Hera can be rationalized by an initial, rapid binding of the 32mer hairpin to the RBD, and subsequent binding of the flanking single- or double-stranded region to the helicase core (see Supplementary Fig. S2). To directly test whether the first step described by K_{d1} could reflect binding of the 32mer to the RBD, we measured binding of

Table 3. RNA binding kinetics

(a) 32mer

	RBDs	cores	K_{d1} (μM)	k_2 (s^{-1})	k_{-2} (s^{-1})	K_{d2}	K_d (μM)	$K_{d\,(eq)}$[a] (μM)
# of RBDs								
Hera	2	2	1.7 ± 0.7	173 ± 21	50 ± 9	0.29 ± 0.06	0.49 ± 0.22	0.06 ± 0.01
Hera/Hera_1–419	1	2	2.3 ± 1.5	188 ± 44	66 ± 11	0.35 ± 0.10	0.81 ± 0.64	0.25 ± 0.09
Hera_1–419	0	2	n.d.[b]	n.d.	n.d.	–	–	16 ± 7
# of (functional) cores								
Hera	2	2	1.7 ± 0.7	173 ± 21	50 ± 9	0.29 ± 0.06	0.49 ± 0.22	0.06 ± 0.01
Hera/Hera_K51Q	2	1	0.5 ± 0.2	179 ± 12	46 ± 14	0.26 ± 0.08	0.13 ± 0.07	0.08 ± 0.02
Hera_K51Q	2	0	2.8 ± 1.2	194 ± 32	107 ± 6	0.55 ± 0.09	1.5 ± 0.7	0.17 ± 0.02
Hera_1–419	0	2	n.d.	n.d.	n.d.	–	–	16 ± 7
Hera_1–365	0	1	n.d.	n.d.	n.d.	–	–	81 ± 29
position of RBD								
Hera	2	2	1.7 ± 0.7	173 ± 21	50 ± 9	0.29 ± 0.06	0.49 ± 0.22	0.06 ± 0.01
cis	1	1	0.17 ± 0.08	178 ± 25	18 ± 29	0.10 ± 0.16	0.017 ± 0.03	0.126 ± 0.009
trans	1	1	n.a.[c]	10 ± 1[d]	75 ± 4	–	7.3 ± 1.0	3.1 ± 0.5
cis-like	1	1	n.d.	n.d.	n.d.	–	–	n.d.
trans-like	1	1	n.d.	n.d.	n.d.	–	–	n.d.
RBD	1	1	n.d.	12.5 ± 0.4[d]	34 ± 0.7	–	2.7 ± 0.014	1.0 ± 0.2

(b) 32/9mer

	RBDs	cores	K_{d1} (μM)	k_2 (s^{-1})	k_{-2} (s^{-1})	K_{d2}	K_d (μM)	$K_{d\,(eq)}$[a] (μM)
Hera	2	2	5 ± 1.5	224 ± 33	134 ± 6	0.59 ± 0.09	3.0 ± 1.0	2.0 ± 0.3
cis	1	1	4 ± 1.9	262 ± 28	103 ± 17	0.40 ± 0.08	1.8 ± 0.8	1.4 ± 0.5

[a] K_d value from equilibrium titrations (see Table 2).
Hera concentrations are given as dimer concentrations. K_{d1}, K_{d2}, K_d, and $K_{d\,(eq)}$ therefore need to be multiplied by the number of protomers for comparisons.
[b] n.d.: not determined
[c] n.a.: not applicable
[d] bimolecular reaction, unit μM s^{-1}.
Errors are the errors of the concatenated fit of the cumulative data from at least two independent experiments.

the isolated RBD (Hera_424–510) to the fl-32mer in stopped-flow experiments. Binding of the RBD also led to a single-exponential increase in fluorescence, demonstrating that this step is associated with a change in signal. The k_{obs} showed a linear dependence on the concentration of the RBD in the concentration range tested. Such a linear dependence may indicate a lack of saturation, meaning we only sampled the linear part of a hyperbolic dependence. Alternatively, it could point to a one-step binding mechanism. In this case, the rate constants for binding and dissociation, k_1 and k_{-1}, are determined by the slope and *y*-intercept of the linear dependence (Equation 10), which gives $k_1 = 12.5 \pm 0.4$ μM^{-1} s^{-1} and $k_{-1} = 34 \pm 0.7$ s^{-1} (Supplementary Fig. S4), corresponding to $K_{d1} = 2.7 \pm 0.014$ μM. This value is in good agreement with the K_{d1} value per protomer determined for the Hera dimer ($K_{d1} = 3.4 \pm 1.4$ μM) and the value for Hera/Hera_1–419 heterodimer ($K_{d1} = 2.3 \pm 1.5$ μM), supporting the assignment of the first step as binding of the hairpin to the RBD.

The overall K_d values for the 32mer complexes of Hera, Hera/Hera_1–419, and Hera_1–419 from kinetic data rank the proteins in the same order of 32mer affinities that were determined in equilibrium titrations (Hera < Hera/Hera_1–419 << Hera_1–419), although the absolute values differ. This difference could simply be due to the different signals measured (fluorescence anisotropy versus intensity). It could also indicate that slower processes such as slow isomerization steps not detected by stopped flow may contribute to binding. It is also conceivable that the two-step binding model, with a signal change in the first binding step and a spectroscopically silent second step, does not faithfully recapitulate all features of the underlying binding mechanism. For example, binding to the two cores and/or the RBDs could occur with different affinities and/or with different changes in signal. In fact, the observed increase in fluorescence on binding of the 32mer to the isolated RBD indicates that both steps of binding are associated with changes in intensity, and suggests that the two-step model with a change in signal exclusively in the second step is over-simplified.

We also measured binding of Hera to the fl-32/9mer in stopped-flow experiments (Fig. 2F, Table 3 (b)). Again, the stopped-flow traces showed a rapid increase in intensity that could be described by single-exponential functions. From the hyperbolic dependence of k_{obs} on the concentration of Hera, again consistent with two-step binding, we obtained $K_{d1} = 5 \pm 1.5$ μM, $k_2 = 224 \pm 33$ s^{-1}, and $k_{-2} = 134 \pm 6$ s^{-1} ($K_{d2} = 0.59 \pm 0.09$, $K_d = 3.0 \pm 1.0$ μM). The overall K_d value reflects the lower affinity of Hera for the 32/9mer than for the 32mer detected in equilibrium titrations.

The stopped-flow data on RNA binding support all main observations from equilibrium titrations: Hera interacts more tightly with the 32mer than with the 32/9mer. Removal of the RBDs weakens binding of Hera to the 32mer. Removing one of the two RBDs has a moderate effect, removing both RBDs substantially weakens 32mer binding.

Connecting equilibrium and kinetic data

With the insight from the kinetic analyses that RNA binding to Hera follows a two-step binding model, we re-analyzed the titration data for Hera with a two-step binding model using Dynafit (Supplementary Fig. S5A, Dynafit Script 3, see Supplementary data for a more detailed description of Dynafit analyses). The equilibrium data are reasonably well-described with the parameter set obtained from the analysis of the hyperbolic dependence of k_{obs} on Hera concentration for the 32mer (Supplementary Fig. S5B) and for the 32/9mer (Supplementary Fig. S5C). However, the system becomes underdetermined when all parameters are varied, with large correlations between parameters, precluding an independent determination of these values from equilibrium data. Nevertheless, these comparisons show that the equilibrium and kinetic data are consistent and support a two-step binding model for the interaction of Hera with the 32mer and 32/9mer.

We next challenged this model by describing the titration data for Hera/Hera_1–419 with two-step binding to the Hera protomer and one-step binding to the Hera_1–419 protomer Supplementary Fig. S5D, Dynafit Script 4a). The simulated data with values for K_{d1}, k_2, and k_{-2} obtained from the hyperbolic dependence of k_{obs} on the concentration of Hera (Table 3 (a)), and a K_d obtained from the Dynafit analysis using a one-step binding model for Hera_1–419 (as no concentration dependence of k_{obs} was observed to determine k_1 and k_{-1}) reasonably described the experimental data (Supplementary Fig. S5E). When individual or several parameters were varied, the curves matched the data more closely, but the parameters were returned with large errors, indicating that the system is underdetermined and the quantitative analysis not possible.

The simulation of the 32/9mer titration with Hera/Hera_1–419 according to the one-step-/two-step binding model (see Dynafit script 4a), with kinetic parameters for Hera [Table 3(b)] and the K_d from the Dynafit analysis (Table 2) for Hera_1–419, also matches the overall shape of the experimental curve (Supplementary Fig. S5F). Varying one or several parameters gives curves that match the experimental data, but the parameters are affected by large errors; the system is underdetermined.

Overall, titration and kinetic data are thus consistent with one-step binding of 32mer and 32/9mer to the isolated RBD (and, by inference, to the isolated helicase core), and with two-step binding to Hera, with a rapid interaction of the hairpin with the RBD in the first step, and a subsequent, slower interaction of the flanking region with the helicase core.

RNA unwinding

Our data show that the RBDs are a key element for the initial interaction of Hera with RNA and play a (minor) role in RNA-stimulated ATPase activity. Next, we asked whether the number of RBDs present also affects Hera-mediated RNA unwinding. Duplex unwinding was followed as a function of time under single-turnover conditions, using a Cy3/Cy5-labeled 32/9mer as a substrate and the decrease in FRET as a probe (Fig. 2G, Supplementary Fig. S1C, and Table 4). Reactions in the absence of ATP were performed as a negative control.

RNA unwinding by Hera, Hera/Hera_1–419, and Hera_1–419 occurred on the minute time scale, and was thus much slower than RNA binding (Supplementary Fig. S1C), indicating that steps subsequent to binding are rate-limiting for unwinding. Unwinding traces were described by single-exponential functions to extract the observed rate constant k_{obs}. The observed rate constants showed a hyperbolic dependence on the concentration of Hera (Fig. 2G), pointing to contributions from RNA binding. Although binding of RNA to the RBDs occurs on a much faster time scale, the concentrations of Hera used in these experiments range from subsaturating to saturating, rationalizing the observed concentration dependence. By analyzing the concentration dependence of k_{obs} using Equation (11), an unwinding rate constant at saturation of $k_{unw} = 0.062 \pm 0.008$ s^{-1} and a concentration required for half-maximal unwinding rate of $K_{1/2,unw,} = 1.4 \pm 0.4$ μM were determined for the Hera dimer (Table 4). $K_{1/2,unw}$ per protomer is again twice the value determined, i.e. $K_{1/2,unw} = 2.9$ μM per protomer, which puts it into the range of the RBD affinity for RNA, whereas k_{unw} is concentration-independent.

Table 4. RNA unwinding

	RBDs	cores	$K_{1/2,unw}$ (μM)	k_{unw} (s^{-1})
# of RBDs				
Hera	2	2	1.4 ± 0.4	0.062 ± 0.008
Hera/Hera_1–419	1	2	2.6 ± 1.4	0.016 ± 0.003
Hera_1–419	0	2	1.2 ± 0.4	0.0062 ± 0.0007
# of (functional) cores				
Hera	2	2	1.4 ± 0.4	0.062 ± 0.008
Hera/Hera_K51Q	2	1	2.0 ± 0.8	0.019 ± 0.003
Hera_K51Q	2	0	n.d.[a]	n.d.
Hera_1–419	0	2	1.3 ± 0.4	0.0062 ± 0.0007
Hera_1–365	0	1	2.3 ± 0.6	0.0016 ± 0.0001
position of RBD				
Hera	2	2	1.4 ± 0.4	0.062 ± 0.008
cis	1	1	2.5 ± 0.8	0.015 ± 0.002
trans	1	1	4 ± 3.0	0.022 ± 0.008
cis-like	1	1	8.7 ± 3.9	0.012 ± 0.003
trans-like	1	1	2 ± 1.1	0.009 ± 0.002

Hera concentrations are given as dimer concentrations. $K_{1/2,unw}$ therefore reflects the value for the number of unwinding units present.
[a]n.d.: not detected.
Errors are the errors of the concatenated fit of the cumulative data from at least two independent experiments.

Hera/Hera_1–419 (one RBD) showed a 4-fold lower rate constant of $k_{unw} = 0.016 \pm 0.003$ s^{-1} and an unwinding constant of $K_{1/2,unw} = 2.6 \pm 1.4$ μM (Table 4). The value for $K_{1/2,unw}$ is in good agreement with the value determined per protomer for Hera ($K_{1/2,unw} = 2.9$ μM). The rate constant of unwinding, k_{unw}, contains contributions from unwinding by the core of the Hera protomer carrying the RBD ($k_{unw} = 0.031$ s^{-1}) and the core of Hera_1–419 lacking an RBD. For Hera_1–419 (no RBD), unwinding was very slow, with $k_{unw} = 0.0062 \pm 0.0007$ s^{-1} ($K_{1/2,unw} = 1.2 \pm 0.4$ μM), demonstrating that the unwinding by Hera/Hera_1–419 is caused predominantly, if not exclusively, by the Hera protomer.

ATP- and RNA-induced conformational changes: single-molecule FRET experiments

The Hera helicase core switches from an open state to a closed state on binding of RNA and ATP [8]. This conformational change can be observed as an increase in FRET efficiency between dyes attached to the N-terminal and C-terminal RecA

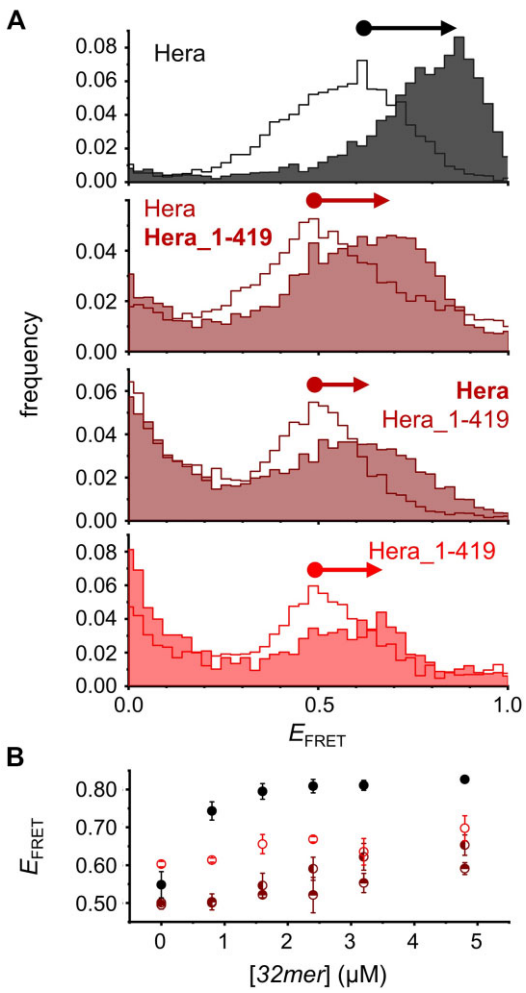

Figure 3. Effect of the RBDs on the conformational change of the helicase core. (**A**) Single-molecule FRET histograms for donor/acceptor-labeled Hera (black), Hera/Hera_1–419 (brown), and Hera_1–419 (red) in the absence (lines, no fill) or presence of 5 mM ADPNP and 32mer RNA (lines, colored fill). The RNA concentration was 4.8 μM (Hera, Hera/Hera_1–419) or 3.2 μM (Hera_1–419). For Hera/Hera_1–419, either the core of Hera or the core of Hera_1–419 was labeled; the labeled protomer is highlighted in bold. Data for Hera_1–419 were measured after subunit exchange with a 5-fold molar excess of unlabeled protein to ensure the formation of homodimers with only one labeled core (see Supplementary Fig. S6 for a comparison of this histogram with the histogram of the homodimer with four cysteines). Histograms are representative histograms from at least two independent experiments. (**B**) Dependence of the FRET efficiency on the concentration of 32mer RNA for donor/acceptor-labeled Hera (black, filled circles), Hera/Hera_1–419 (brown, half-filled circles horizontal: Hera labeled, half-filled circles vertical: Hera_1–419 labeled), and Hera_1–419 (red, open circles) in the presence of 5 mM ADPNP. Error bars reflect the error of the mean from at least two independent experiments.

domains (RecA_N, RecA_C; see Fig. 1A and B). Using single-molecule FRET experiments and Hera variants carrying a donor and acceptor fluorophore in RecA_N (Cys115) and RecA_C (Cys227), we tested whether Hera with two, one, or no RBD(s) responds to RNA and ATP binding (Fig. 3). For Hera/Hera_1–419, with two functional cores but only a single RBD, we either labeled the helicase core on the same protomer as the RBD (*cis*), or the helicase core on the other protomer lacking an RBD (*trans*; see Section "Cooperation of the RBDs with the helicase cores: heterodimers with one functional core and one RBD in *cis* or *trans*").

Donor–acceptor-labeled Hera_E115C_E227C showed a FRET efficiency of $E_{FRET} \approx 0.6$ in the absence of ligands that increased to $E_{FRET} \approx 0.85$ on addition of 32mer and the nonhydrolyzable ATP analog ADPNP (Fig. 3A). This increase in FRET efficiency is indicative of closing of the helicase core [8]. Hera/Hera_1–419, labeled in *cis* or in *trans* relative to the single RBD present, showed a narrower distribution of FRET efficiencies, with $E_{FRET} \approx 0.5$ in the apo-state. The more defined histogram is the result of the presence of only two cysteines in Hera/Hera_1–419, and hence a single distance between donor and acceptor fluorophores. In contrast, the Hera dimer contains four cysteines, and labeling with donor and acceptor dyes leads to a heterogeneous mixture of species carrying the two dyes in different positions [115–227 (same protomer), 115–227 (different protomers), 115–115, and 227–227], resulting in different donor/acceptor distances and different FRET distributions that are superimposed in the overall histogram. Addition of RNA and ADPNP to Hera/Hera_1–419 resulted in the appearance of a high-FRET state at $E_{FRET} \approx 0.65$–0.7, irrespective of which core was labeled. Hence, both cores in Hera/Hera_1–419 can close on binding of RNA and ADPNP, independent of the relative position of the RBD. Note that the RNA is in large excess and present in high concentrations in these experiments. It is conceivable that, at these concentrations, it may directly bind to the core of the Hera_1–419 protomer, causing it to close. The FRET histogram of Hera_1–419 (no RBD) showed a broad peak at $E_{FRET} \approx 0.6$ that increased slightly to $E_{FRET} \approx 0.65$ on addition of ADPNP and RNA (Supplementary Fig. S6). Again, the broad histogram is the result of the four cysteines present, and the contributions of different species with different donor/acceptor distances formed on statistical labeling. As this broad distribution may preclude the detection of a change in FRET efficiency, we generated a Hera_1–419 heterodimer from a protomer with two cysteines and a cysteine-free protomer. This heterodimer showed a well-defined FRET histogram with $E_{FRET} \approx 0.5$ in the apo-state and exhibited a clear shift to $E_{FRET} \approx 0.65$–0.7 on addition of ADPNP and 32mer (Fig. 3A), confirming that the helicase core closes on direct binding of RNA and ADPNP. This is consistent with closing of the (monomeric) Hera helicase core on binding of poly-U RNA and ADPNP as reported previously [8].

The FRET efficiencies as a function of 32mer concentration (Fig. 3B) reflect the reduced affinities of Hera/Hera_1–419, and Hera_1–419 compared to Hera for the 32mer, as observed in anisotropy titrations (see Fig. 2C).

Altogether, these experiments demonstrate that the helicase core of Hera closes on binding of RNA and ADPNP even in the absence of the RBDs, indicating that the RBDs are not necessary for closing. However, their presence favors formation of the closed state at lower concentrations of 32mer, consistent with their contribution to RNA binding.

Overall, these experiments are consistent with Hera binding the 32mer by initial interactions of the RBD with the hairpin, followed by interactions of the core with the adjacent duplex. In the presence of ATP, the interaction of RNA with the core leads to core closing, independent of the interactions of the RNA with the RBD, and to unwinding of the duplex by the core. The reduction in the rate constant of unwinding under saturating conditions observed for Hera/Hera_1–419 (Fig. 2G and Table 4) suggests an appreciable effect of deleting

one RBD on cooperativity between the protomers in RNA unwinding. A similar effect is seen for RNA-stimulated ATPase activity in the presence of poly-U RNA (Fig. 2B and Table 1), but not for closing of the helicase core.

Role of the cores: Hera containing two or one functional helicase core(s)

To dissect the role of the two helicase cores for RNA unwinding by Hera, we compared the RNA-stimulated ATPase activity, RNA binding and unwinding, and conformational changes of Hera containing one or two functional helicase cores. To probe the role of the two cores in the presence of the RBDs, we compared Hera (two functional cores, two RBDs) with a heterodimer generated from one copy of Hera and one copy of Hera_K51Q, carrying a mutation in the Walker A motif (motif I) that renders it ATPase- and unwinding-deficient (one functional core, two RBDs; Figs 1A and C, and 4A). The Hera_K51Q dimer served as a negative control (no functional core, two RBDs). To address the role of the two helicase cores in the absence of the RBDs, we compared the properties of the dimeric core (Hera_1–419) with the monomeric core (Hera_1–365; Figs 1C and 5A; [8]).

RNA-stimulated ATPase activity

Again, we first assessed the effect of the cores on the RNA-dependent ATPase activity (Fig. 4B, Supplementary Fig. S7A, and Table 1). Hera_K51Q (no functional core, two RBDs) did not show any ATPase activity (Fig. 4B). Hera/Hera_K51Q (one functional core, two RBDs) had a turnover number k_{cat} of 1.19 ± 0.05 s^{-1} and $K_{1/2,RNA}$ of 109 ± 18 μM. The turnover number is about half of the corresponding values determined for Hera (k_{cat} = 2.3 ± 0.3 s^{-1}), as expected from inactivation of one helicase core in the dimer (in the absence of cooperativity). The $K_{1/2,RNA}$ of 109 ± 18 μM is also half of the value for Hera (240 ± 84 μM; see Table 1). As a result, the catalytic efficiency $k_{cat}/K_{1/2,RNA}$ of 0.009 ± 0.002 μM^{-1} s^{-1} of Hera/Hera_K51Q is identical to that of Hera ($k_{cat}/K_{1/2,RNA}$ = 0.009 ± 0.003 μM^{-1} s^{-1}).

In the absence of the RBDs, the effect of the number of cores can be gleaned from the comparison of Hera_1–365 and Hera_1–419 (monomeric and dimeric cores; Figs 1C and 5A). We showed before that Hera_1–419 (two cores, no RBD) has a reduced turnover number k_{cat} of 0.9 ± 0.3 s^{-1} compared to Hera (2.3 ± 0.3 s^{-1}), but a higher $K_{1/2,RNA}$ of 871 ± 552 μM (240 ± 84 μM for Hera, see Table 1), in agreement with a lower RNA affinity of the core. The catalytic efficiency of $k_{cat}/K_{1/2,RNA}$ of 0.001 ± 0.0008 μM^{-1} s^{-1} is ∼9-fold reduced compared to Hera (0.009 ± 0.003 μM^{-1} s^{-1}). For Hera_1–365 (one core, no RBD), no RNA-dependent ATPase activity was detected (Fig. 5B and Supplementary Fig. S7A). These data suggest that dimerization is important for RNA-stimulated ATPase activity of the Hera core in the absence of the RBDs.

Together, these data show that the inactivation of one of the cores in Hera does not significantly affect the RNA-stimulated ATPase activity of the other core. In the absence of the RBDs, both cores seem to cooperate in RNA-dependent ATP hydrolysis.

RNA affinity

We next tested the effect of the number of (active) cores on RNA binding in fluorescence equilibrium titrations and stopped-flow experiments (Figs 4C and D, and 5C; Supplementary Fig. S7B; and Table 2). By analyzing the titration curves with Equation (4), we obtained K_d values for Hera/Hera_K51Q (one functional core, two RBDs) of K_d = 0.08 ± 0.02 μM (32mer; Fig. 4C and Table 2) and K_d = 2.5 ± 0.4 μM (32/9mer; Fig. 4D). For Hera_K51Q, the values were K_d = 0.17 ± 0.02 μM (32mer; Fig. 4C) and 2.1 ± 0.4 μM (32/9mer; Fig. 4D). Thus, the affinities of Hera_K51Q for the 32mer and 32/9mer are comparable to Hera [K_d = 0.06 ± 0.01 μM (32mer) and 2.3 ± 0.3 μM (32/9mer); see Table 2].

Numerical analyses with Dynafit, based on a one-step binding model and independent, non-cooperative binding to the two protomers (see Dynafit Script 1; Supplementary Fig. S8), were again virtually identical to the ones determined per protomer by analysis with Equation (4) (see Table 2). When we tested analysis of the Hera_K51Q titrations of 32mer and 32/9mer with a cooperative binding model (see Dynafit Script 2), K_{d1} and K_{d2} for the two binding events were again highly correlated, precluding their determination.

When we used the parameters for the Hera and Hera_K51Q homodimers determined from the numerical analyses to describe the experimental data for the titration of the 32mer and 32/9mer with the Hera/Hera_K51Q heterodimer (see Dynafit Script 2b), the resulting binding curves only roughly described the experimental data (Supplementary Fig. S8A). When K_{d1} and K_{d2} were varied, their high correlation again precluded their independent determination from the fits, both for the 32mer and for the 32/9mer titrations (see Supplementary data for a more detailed description of the Dynafit analyses).

Collectively, the titration data demonstrate that the K51Q mutation has essentially no effect on binding of Hera to the 32/9mer and little effect on binding of the 32mer (Table 2). Similar to the effect of the RBDs, the effect of the number of cores on RNA affinity was more pronounced for the 32mer, while the affinity for the 32/9mer was virtually independent of the number of functional cores. In contrast to the RBDs, the effect of inactivating one core was similar to the effect of inactivating the second core. These observations are consistent with RNA binding by the RBDs, with little contribution from the core in the absence of ATP.

The requirement of the RBDs for RNA binding was also evident when we compared the effect of the number of cores on RNA affinities in the absence of the RBDs. Hera_1–419 (two cores, no RBD) had increased K_d values of 16 ± 7 μM (32mer) and 11 ± 5 μM (32/9mer; see Table 2; K_d values per core are again twice these values). For Hera_1–365 (one core, no RBD), the affinity for the 32mer was decreased much further, to 81 ± 29 μM (Fig. 5C), which would rationalize the lack of RNA-stimulated ATPase activity (see Fig. 5B).

Overall, the RNA affinities of Hera and Hera_K51Q are similar, the absence of the RBDs is associated with markedly reduced RNA affinities, and the apparent RNA affinity is significantly higher with two cores, at least when the RBDs are absent.

RNA binding kinetics

While the RNA affinity is not affected much by the functionality of the helicase core, we also tested whether the kinetics of RNA binding are different for Hera with two, one, or no functional helicase core(s) in stopped-flow experiments. First, we compared Hera (two functional cores,

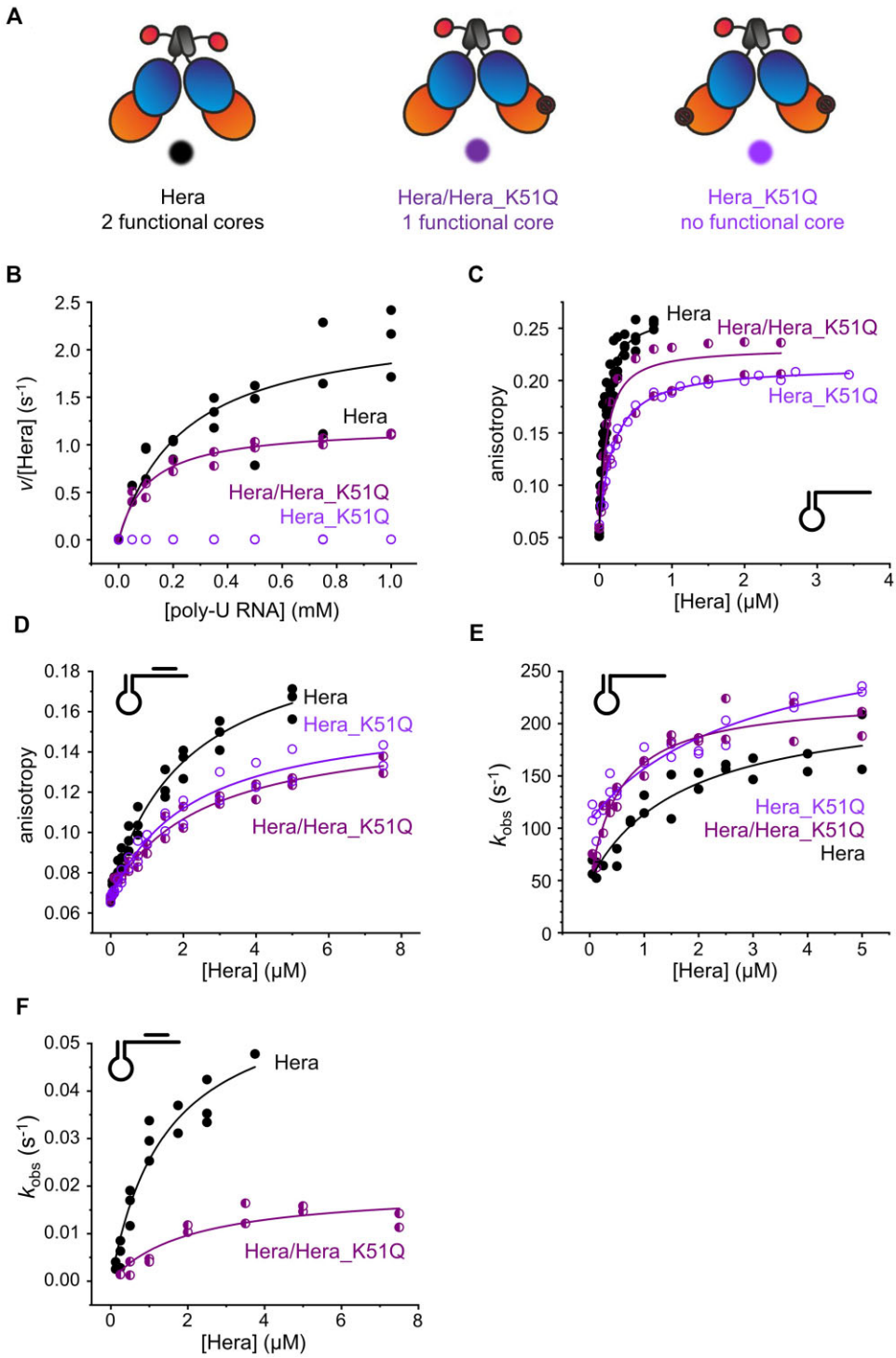

Figure 4. Effect of inactivation of one or two helicase cores on RNA-stimulated ATPase activity, RNA binding and unwinding in the presence of the RBDs. (**A**) Hera constructs with two RBDs and two, one, or no functional core: Hera (two cores, two RBDs; black), Hera/Hera_K51Q (heterodimer, one functional core, two RBDs; dark purple), and Hera_K51Q (dimeric core: two cores, no RBD; purple). (**B**) RNA-dependent ATPase activity of 0.15 μM of Hera (two cores, black; filled circles; same data as in Fig. 2B) and 0.30 μM of Hera/Hera_K51Q (one functional core; dark purple, half-filled circles). Data are cumulative data points from at least two independent experiments. The lines are cumulative fits to all data points with the Michaelis–Menten equation (see "Materials and methods" section). See Supplementary Fig. S7A for original data. (**C**) Fluorescence equilibrium titrations of 32mer with Hera (black, filled circles; same data as in Fig. 2C), Hera/Hera_K51Q (dark purple, half-filled circles), and Hera_K51Q (purple, open circles). Lines are fits according to a 1:1 binding model (see "Materials and methods" section). (**D**) Fluorescence equilibrium titrations of 32/9mer with Hera (black, filled circles; same data as in Fig. 2D), Hera/Hera_K51Q (dark purple, half-filled circles), and Hera_K51Q (purple, open circles). Lines are fits according to a 1:1 binding model (see "Materials and methods" section). (**E**) Concentration dependence of observed rate constants k_{obs} for binding of Hera (black, filled circles; same data as in Fig. 2E), Hera/Hera_K51Q (dark purple, half-filled circles), and Hera_K51Q (purple, open circles) to 32mer RNA. Rate constants were obtained by describing stopped-flow traces (see Supplementary Fig. S7B) with single-exponential functions. (**F**) Concentration dependence of observed rate constants k_{obs} for 32/9mer unwinding by Hera (black, filled circles; same data as in Fig. 2G) and Hera/Hera_K51Q (dark purple, half-filled circles). Rate constants were obtained by describing fluorescence traces (see Supplementary Fig. S7C) with single-exponential functions.

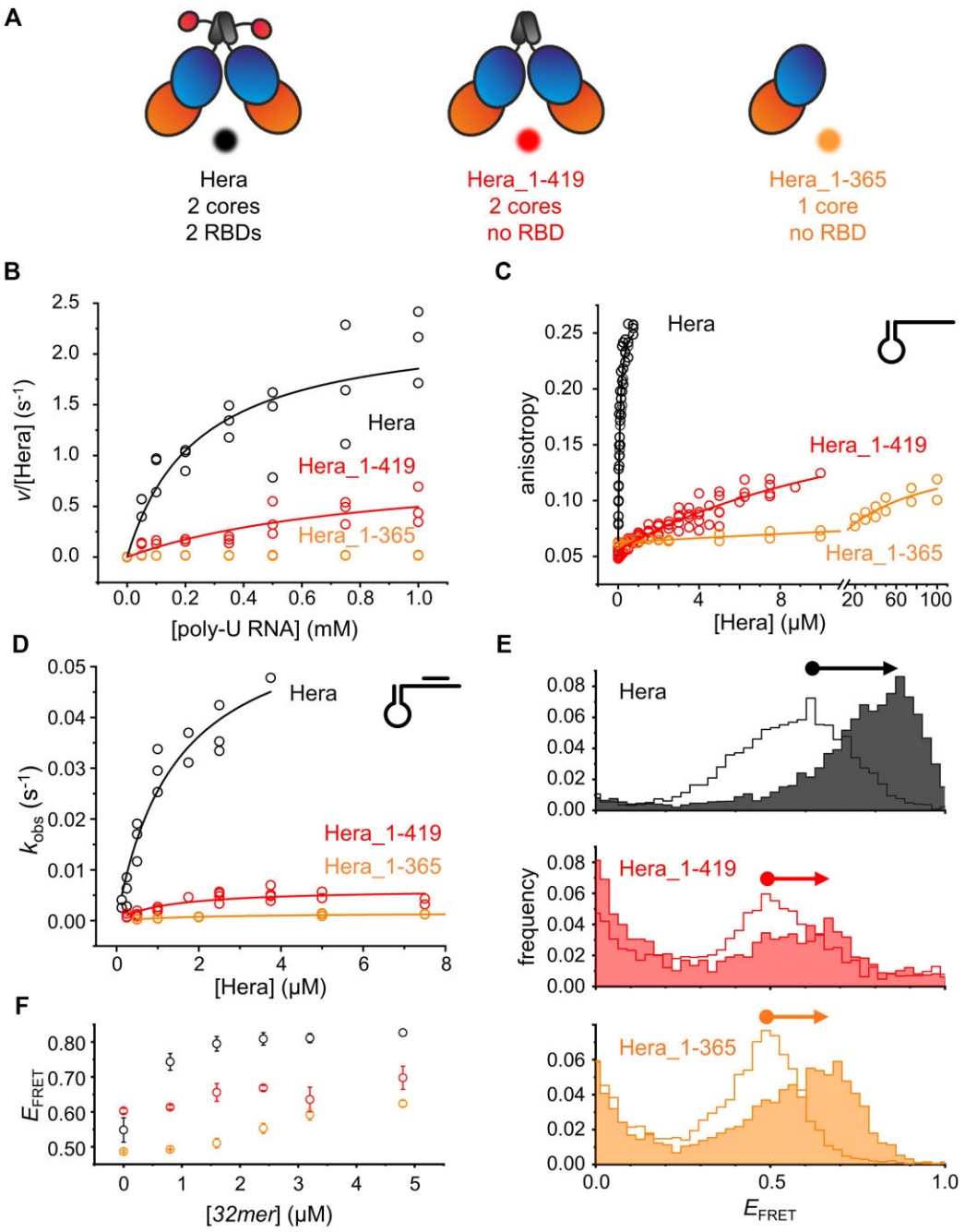

Figure 5. Effect of the number of helicase cores on RNA-stimulated ATPase activity, RNA binding and unwinding, and conformational changes of the helicase core in the absence of the RBDs. (**A**) Hera (two cores, two RBDs; black), Hera_1–419 (dimeric core: two cores, no RBD; red), and Hera_1–365 (monomeric core: one core, no RBD; orange). (**B**) RNA-dependent ATPase activity of 0.15 μM of Hera (black; same data as in Fig. 2B), 0.15 μM of Hera_1–419 (red, same data as in Fig. 2B), and 0.3 μM of Hera_1–365 (orange). Data are cumulative data points from at least two independent experiments. The lines are cumulative fits to all data points with the Michaelis–Menten equation (see "Materials and methods" section). (**C**) Fluorescence equilibrium titrations of 32mer with Hera (black; same data as in Fig. 2C), Hera_1–419 (red; same data as in Fig. 2C), and Hera_1–365 (orange). Lines are fits according to a 1:1 binding model (see "Materials and methods" section). (**D**) Concentration dependence of observed rate constants k_{obs} for 32/9mer unwinding by Hera (black; same data as in Fig. 2G), Hera_1–419 (red; same data as in Fig. 2G), and Hera1-365 (orange). Rate constants were obtained by describing fluorescence traces with single-exponential functions. (**E**) Single-molecule FRET histograms for donor–acceptor-labeled Hera (black; same data as in Fig. 3A), Hera_1–419 (red; same data as in Fig. 3A), and Hera_1–365 (orange) in the absence (lines, no fill) and presence of 5 mM ADPNP and 32mer RNA (4.8 μM with Hera, Hera_1–356, 3.2 μM with Hera_1–419; lines, colored fill). Representative histograms from at least two independent experiments. (**F**) FRET efficiency as a function of the concentration of 32mer RNA for donor–acceptor-labeled Hera (black; same data as in Fig. 3B), Hera_1–419 (red; same data as in Fig. 3B), and Hera_1–365 (orange) in the presence of 5 mM ADPNP. Error bars reflect the error of the mean from at least two independent experiments.

two RBDs), Hera/Hera_K51Q (one functional core, two RBDs), and Hera_K51Q (no functional core, two RBDs; Fig. 4E, Supplementary Fig. S7B, and Table 3). We observed a hyperbolic dependence of k_{obs} for RNA binding on Hera/Hera_K51Q and Hera_K51Q concentrations, suggesting similar two-step binding of RNA as observed for Hera. The K_{d1} is 0.5 ± 0.2 μM for Hera/Hera_K51Q, and increases to 2.8 ± 1.2 μM for Hera_K51Q (Fig. 4E and Table 3). The rate constants for the second binding step were determined as k_2 = 179 ± 12 s^{-1} and k_{-2} = 46 ± 14 s^{-1} for Hera/Hera_K51Q (K_{d2} = 0.26 ± 0.08, K_d = 0.13 ± 0.07 μM), and k_2 = 194 ± 32 s^{-1} and k_{-2} = 107 ± 6 s^{-1} for Hera_K51Q (K_{d2} = 0.55 ± 0.09; K_d = 1.5 ± 0.7μM); the values determined for Hera were K_{d1} = 1.7 ± 0.7 μM, k_2 = 173 ± 21 s^{-1}, and k_{-2} = 50 ± 9 s^{-1} (K_{d2} = 0.29 ± 0.06, K_d = 0.49 ± .022 μM; see Fig. 2E and Supplementary Fig. S1B). The overall K_d values from kinetic data reflect the moderate reduction in RNA affinity observed for Hera_K51Q in equilibrium titrations (Fig. 4C and D). Additional measurements with 32/9mer were therefore not performed.

Again, we used the knowledge on two-step binding of the 32mer to Hera, Hera_K51Q, and Hera/Hera_K51Q to analyze the equilibrium titration data with two-step binding models using Dynafit (Supplementary Fig. S9A and C, see Dynafit Scripts 3a–d). Using different sets of K_{d1}, k_2, and k_{-2} for the Hera protomer and for the Hera_K51Q protomer, determined in the kinetic analysis of the Hera and Hera_K51Q homodimers, gave a simulated curve that describes the data reasonably well (Supplementary Fig. S9D), demonstrating internal consistency of the data. As we lacked kinetic data for 32/9mer binding to Hera/Hera_K51Q and Hera_K51Q, we simulated binding curves for the 32/9mer to Hera_K51Q and Hera/Hera_K51Q with a two-step binding model to test whether we can extract the underlying parameters (see Dynafit Script 3a, Supplementary Fig. S9B and D). The agreement between simulation and data further supports that Hera and Hera_K51Q interact similarly both with the 32mer and with the 32/9mer.

Comparing the kinetics of RNA binding to Hera with two or one functional core(s) in the absence of RBDs was not possible. Hera_1–419 (two cores, no RBD) showed no clear dependence of the observed rate constant on the concentration of Hera (see Fig. 2E). The low RNA affinity of Hera_1–365 (one core, no RBD) precluded stopped flow measurements at reasonable concentrations.

Overall, the inactivation of one or both helicase cores by the K51Q mutation does not affect RNA affinity or binding kinetics much when the RBDs as the major RNA-binding platform are present. In the absence of the RBDs, the helicase core has a much lower RNA affinity, making the difference in affinity between monomeric and dimeric cores difficult to assess. Equilibrium data indicate that two cores lead to an increase in RNA affinity compared to a single core (Fig. 5C and Table 2).

RNA unwinding

We next tested the role of the two cores for RNA unwinding, again both in the presence and absence of the RBDs (Figs 4F and 5D; Supplementary Figs S1C and S7C; Table 4). Hera/Hera_K51Q (one functional core, two RBDs) showed RNA unwinding with k_{unw} = 0.019 ± 0.003 s^{-1}, ~3-fold more slowly than Hera (k_{unw} = 0.062 ± 0.008 s^{-1}), suggesting that inactivation of one core reduces the unwinding activity of the remaining functional core (Fig. 4F and Table 4). $K_{1/2,unw}$ for the functional core in Hera/Hera_K51Q was similar to Hera, with $K_{1/2,unw}$ = 2.0 ± 0.8 μM (1.4 ± 0.4 μM for Hera), in agreement with the negligible effect of the K51Q mutation on RNA affinities. Hera_K51Q (no functional core, two RBDs) did not show unwinding activity.

In the absence of the RBDs, the two cores of Hera_1–419 (two cores, no RBDs) supported RNA unwinding with a rate constant k_{unw} = 0.0062 ± 0.0007 s^{-1} (Fig. 5D, see also Fig. 2G), ~10-fold lower than the rate constants for RNA unwinding by Hera. Hera_1–365 (one core, no RBDs) unwinds RNA with an even lower rate constant of k_{unw} = 0.0016 ± 0.0001 s^{-1} (Fig. 5D), confirming that the monomeric core does bind 32/9mer RNA in the presence of ATP, despite the low affinity for this RNA in the absence of ATP. Deletion of one core in the absence of the RBDs thus is associated with a 4-fold reduction of the unwinding rate constant, similar to the effect of inactivating one of the cores in the presence of the RBDs. The concentration dependence of the unwinding rate constants was similar, with $K_{1/2,unw}$ = 2.4 ± 0.8 μM for Hera_1–419 (dimeric core, per core), and $K_{1/2,unw}$ = 2.3 ± 0.6 μM (monomeric core). Thus, the interaction with RNA in the presence of ATP during unwinding is not affected by dimerization.

ATP- and RNA-induced conformational changes: single-molecule FRET experiments

Finally, we also tested whether the number of cores present affected the ATP- and RNA induced activation and closing of the (functional) helicase core in the absence of the RBDs (Hera_1–419, Hera_1–365; Fig. 5E and F). Similar to Hera_1–419_E115C_E227C (two cores, no RBDs; see Fig. 3A and Supplementary Fig. S6), the histogram of Hera_1–365_E115C_E227C (one core, no RBD) showed a distinct peak at E_{FRET} ≈ 0.5 and a clear shift on addition of RNA and ADPNP to E_{FRET} ≈ 0.65–0.7 (Fig. 5E). Collectively, these data demonstrate that neither the presence of the RBDs nor dimerization are prerequisites for closing of the Hera helicase core. The dependence of the FRET efficiency of the high-FRET, closed state on the concentration of the 32mer reflects the reduced 32mer affinities of Hera_1–419 and Hera_1–365 compared to Hera (Fig. 5F).

In summary, we do not observe strong evidence for cooperation of the two helicase cores of the Hera dimer in RNA-stimulated ATP hydrolysis or RNA binding. The RNA- and ATP-induced closing of the helicase core also occurs irrespective of the number of cores present. In contrast, inactivation or removal of one core reduces the RNA unwinding activity of the remaining core.

Cooperation of the RBDs with the helicase cores: heterodimers with one functional core and one RBD in *cis* or *trans*

So far, our data show that a single helicase core of Hera can interact with RNA and nucleotide and undergo a conformational change into a closed state in the presence of these ligands. RNA substrates are bound in a two-step process; they initially interact with the RBD, which facilitates the interaction of flanking regions with the core, leading to stimulation of the ATPase activity and RNA unwinding. Although we observe beneficial effects of two RBDs and two cores for

RNA binding and unwinding, our data suggest that Hera with a single RBD and a single core should be an efficient ATP-dependent RNA helicase. However, it remains unclear whether RNA anchored to the RBD of one protomer can interact only with the core on the same protomer, or also with the core of the second protomer.

To further dissect the cooperation of the two RBDs with the two helicase cores of Hera, we generated heterodimers of Hera that contain one (functional) helicase core and a single RBD that is either part of the same protomer that provides the helicase core (*cis*- or *cis*-like heterodimer) or part of the second protomer that does not contain a (functional) helicase core (*trans*- or *trans*-like heterodimer). To this end, we used two different strategies. First, we generated a *cis*-heterodimer formed by Hera and Hera_208–419, comprising the RecA_C and DD domains, and a *trans*-heterodimer formed by Hera_1–419, comprising the core and the DD, and Hera_370–510, comprising the DD and the RBD (Figs 1C and 6A). The presence of RecA_C in the *cis*-heterodimer was necessary to stabilize the dimerization domain, which we could not produce separately. The RecA_C domain does not contribute to RNA binding. In the second approach, we used Hera/Hera_1–419, a heterodimer with two cores and one RBD, as a scaffold, and inactivated either the core of the Hera_1–419 protomer lacking the RBD (*cis*-like heterodimer) or the core of the Hera protomer containing the RBD (*trans*-like heterodimer, Fig. 6A) by the K51Q mutation. We then compared the ATPase activities, RNA binding and unwinding, and conformational changes of the helicase core of these heterodimers with Hera (Fig. 6).

RNA-stimulated ATPase activity

The *cis*-, *cis*-like, *trans*-, and *trans*-like heterodimers showed a hyperbolic dependence of the reaction velocity on the concentration of poly-U RNA (Fig. 6B and Supplementary Fig. S10A). The k_{cat} values at saturating RNA concentrations were 1.2 ± 0.1 s^{-1} and 0.3 ± 0.09 s^{-1} for the *cis*- and *cis*-like heterodimers, and 1.9 ± 0.4 s^{-1} and 0.7 ± 0.2 s^{-1} for the *trans*- or *trans*-like heterodimers (Table 1), compared to k_{cat} = 2.3 ± 0.2 s^{-1} for Hera (two RBDs), and k_{cat} = 1.0 ± 0.1 s^{-1} for Hera/Hera_1–419 (one RBD). The $K_{1/2,RNA}$ value for the *cis*-heterodimer ($K_{1/2,RNA}$ = 200 ± 52 μM) was similar to Hera (240 ± 84 μM). For the *cis*-like ($K_{1/2,RNA}$ = 519 ± 357 μM), *trans*- ($K_{1/2,RNA}$ = 697 ± 227 μM), and *trans*-like heterodimers ($K_{1/2,RNA}$ = 1113 ± 486 μM; Table 1), the values were not well-determined, but consistent with an increased $K_{1/2,RNA}$. The resulting catalytic efficiencies of all variants were reduced compared to Hera ($k_{cat}/K_{1/2,RNA}$ = 0.009 ± 0.003 μM^{-1} s^{-1}) but to different extents. For the *cis*-heterodimer, the catalytic efficiency decreased 1.5-fold ($k_{cat}/K_{1/2,RNA}$ = 0.006 ± 0.002 μM^{-1} s^{-1}), for the *trans*-heterodimer 3-fold ($k_{cat}/K_{1/2,RNA}$ = 0.003 ± 0.001 μM^{-1} s^{-1}). The catalytic efficiencies of the *cis*- and *trans*-like heterodimers, with two cores present, but only a single functional core, showed 15-fold reduced catalytic efficiencies, with $k_{cat}/K_{1/2,RNA}$ = 0.0006 ± 0.0004 μM^{-1} s^{-1} (*cis*-like) and $k_{cat}/K_{1/2,RNA}$ = 0.0006 ± 0.003 $\mu M^{-1} \cdot s^{-1}$ (*trans*-like). Note that the poly-U RNA used in these experiments interacts directly with the core. Hence, no conclusions can be made regarding the cooperation of the single RBD with the core(s).

RNA affinity

Next, we analyzed the effect of the relative position of the RBD toward the helicase core on RNA binding in fluorescence equilibrium titrations of 32mer and 32/9mer as described (Fig. 6C and D). From equilibrium titrations of the 32mer with the *cis*- and *trans*-heterodimers, we obtained K_d values of K_d = 0.126 ± 0.009 μM (*cis*, 32mer) and K_d = 1.4 ± 0.5 μM (*cis*, 32/9mer), or K_d = 3.1 ± 0.5 μM (*trans*, 32mer) and K_d = 16 ± 6 μM (*trans*, 32/9mer; Fig. 6C and D). For comparison, we also determined the RNA affinities of the isolated RBD [K_d = 1.0 ± 0.2 μM (32mer) and K_d = 17 ± 3 μM (32/9mer; Table 2)]. The *cis*-heterodimer thus binds RNA with comparable affinities to Hera. In contrast, the affinities of the *trans*-heterodimer are reduced 52- and 8-fold compared to Hera, resulting in RNA affinities similar to the isolated RBD. Thus, the helicase core and the RBD can functionally cooperate in RNA binding when they are located on the same protomer. When they are on different protomers, their interaction is strongly disfavored.

RNA binding kinetics

We also tested whether the kinetics of RNA binding are dependent on the relative orientation of the RBD toward the helicase core (Fig. 6E and F, Supplementary Fig. S10B and Table 3). The *cis*-heterodimer showed a hyperbolic concentration dependence of k_{obs}, giving K_{d1} = 0.17 ± 0.08 μM, k_2 = 178 ± 25 s^{-1}, and k_{-2} = 18 ± 29 s^{-1} (K_{d2} = 0.1 ± 0.2, K_d = 0.02 ± 0.03 μM), compared to K_{d1} = 1.7 ± 0.7 μM, k_2 = 173 ± 21 s^{-1}, and k_{-2} = 50 ± 9 s^{-1} (K_{d2} = 0.29 ± 0.06 and K_d = 0.49 ± 0.22 μM) for Hera. For the *trans*-heterodimer, the concentration dependence of k_{obs} was linear in the concentration range tested. The linear dependence may indicate a lack of saturation, meaning we only sampled the linear part of a hyperbolic dependence. Alternatively, it could point to a one-step binding mechanism. In this case, we obtain from slope and *y*-axis intercept the values k_1 = 10 ± 1 μM^{-1} s^{-1} and k_{-1} = 75 ± 4 s^{-1} (K_d = 7.3 ± 1.0 μM). These values rank the affinities in the order *cis* > Hera >> *trans*, which reasonably agrees with the ranking from equilibrium titrations (*cis* ≈ Hera >> *trans*). As seen in the equilibrium data, the RNA affinity of the *trans*-heterodimer from kinetic data is similar to the affinity of the RBD, whereas the affinity of the *cis*-heterodimer is similar to Hera.

Due to the generally lower affinities for the 32/9mer, and the reduced RNA affinity of the *trans*-heterodimer, we determined rate constants for 32/9mer binding only for the *cis*-heterodimer (Fig. 6F, Supplementary Fig. S10B). The observed rate constants k_{obs} showed a hyperbolic dependence on the concentration of the *cis*-heterodimer, giving K_{d1} = 4 ± 1.9 μM, k_2 = 262 ± 28 s^{-1}, and k_{-2} = 103 ± 17 s^{-1} (K_{d2} = 0.40 ± 0.08; K_d = 1.8 ± 0.8 μM). These values are comparable to the ones determined for Hera [K_{d1} = 5 ± 1.5 μM, k_2 = 224 ± 33 s^{-1}, and k_{-2} = 134 ± 6 s^{-1} (K_{d2} = 0.59 ± 0.09, K_d = 2.8 ± 1.0 μM), see Fig. 2F], further supporting similar RNA binding of Hera and the *cis*-heterodimer.

The titration data of the 32mer and the 32/9mer with the *cis*- and trans-heterodimers were reasonably well described by a simulated curve with K_{d1}, k_2, and k_{-2} (*cis*) or k_1 and k_{-1} (*trans*) from the analysis of the concentration dependence of k_{obs} (Supplementary Fig. S11, see Supplementary data for

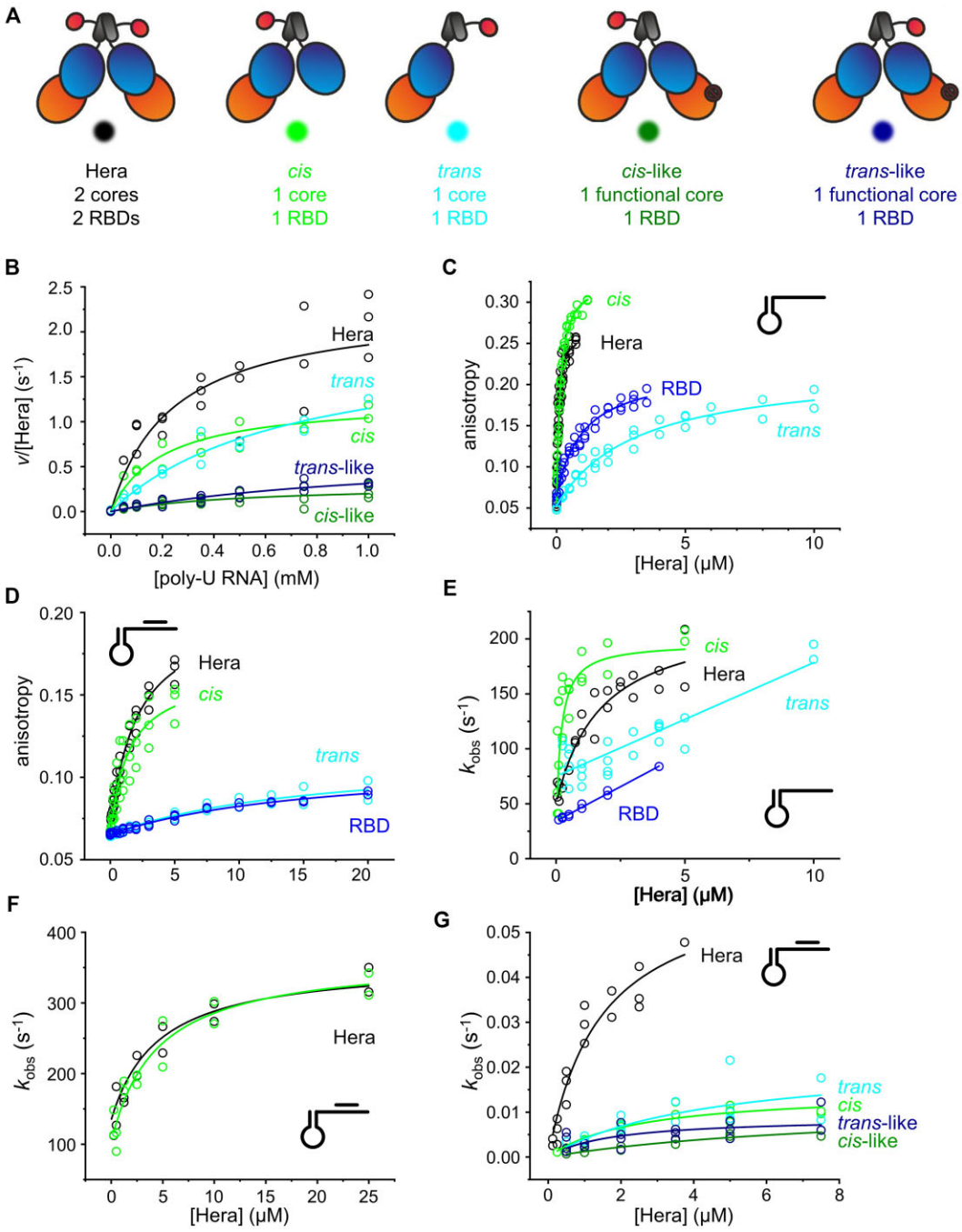

Figure 6. Cooperation of the helicase core(s) with the RBD(s): ATPase activity, RNA binding and unwinding. (**A**) Hera constructs with different relative orientations of the helicase core and a single RBD. Hera (two functional cores, two RBDs; black), the *cis*-heterodimer (one core, 1 RBD in *cis*; green), the *trans*-heterodimer (one core, 1 RBD in *trans*; cyan), the *cis*-like heterodimer (Hera/Hera_1–419_K51Q: one functional core, one RBD in *cis*; dark green), and the *trans*-like heterodimer (Hera_1–419/Hera_K51Q: one functional core, one RBD in *trans*; dark blue). (**B**) RNA-dependent ATPase activity of 0.15 μM of Hera (black; same data set as in Fig. 2B), and 0.30 μM of the *cis*-heterodimer (green), the *trans*-heterodimer (cyan), the *cis*-like heterodimer (dark green), and the *trans*-like heterodimer (dark blue). Data are cumulative data points from at least two independent experiments. The lines are cumulative fits to all data points with the Michaelis–Menten equation (see "Materials and methods" section). See Supplementary Figs S1A and S10A for original data. (**C**) Fluorescence equilibrium titrations of 32mer with Hera (black; same data set as in Fig. 2C), the *cis*-heterodimer (green), the *trans*-heterodimer (cyan), and the RBD (blue). Lines are fits according to a 1:1 binding model (see "Materials and methods" section). (**D**) Fluorescence equilibrium titrations of double-stranded 32/9mer RNA with Hera (black; same data set as in Fig. 2D), the *cis*-heterodimer (green), the *trans*-heterodimer (cyan), and the RBD (blue). Lines are fits according to a 1:1 binding model (see "Materials and methods" section). Hera concentrations are given as concentrations of dimer. (**E**) Concentration dependence of observed rate constants k_{obs} for binding of Hera (black; same data set as in Fig. 2E), the *cis*-heterodimer (green), the *trans*-heterodimer (cyan), and the RBD (blue) to 32mer RNA. Rate constants were obtained by describing stopped-flow traces (see Supplementary Fig. S10B) with single-exponential functions. (**F**) Concentration dependence of observed rate constants k_{obs} for binding of Hera (black) and the *cis*-heterodimer (green) to 32/9mer RNA. Rate constants were obtained by describing stopped-flow traces with single-exponential functions. (**G**) Concentration dependence of observed rate constants k_{obs} for 32/9mer unwinding by Hera (black; same data as in Fig. 2F), the *cis*-heterodimer (green), the *trans*-heterodimer (cyan), the *cis*-like heterodimer (dark green), and the *trans*-like heterodimer (dark blue). Rate constants were obtained by describing the fluorescence traces with single-exponential functions.

a more detailed description of the Dynafit analyses), demonstrating that equilibrium and kinetic data are internally consistent.

Collectively, these data suggest that the communication between the helicase core and the RBD on the same protomer is a key factor for two-step binding of RNA to Hera, at least in the absence of ATP.

RNA unwinding

As the relative position of the RBD to the helicase core determines the cooperation in RNA binding, we also investigated RNA unwinding by the *cis*-, *cis*-like, *trans*-, and *trans*-like heterodimers (Fig. 6G, Supplementary Fig. S10C, and Table 4). All constructs showed a hyperbolic dependence of the observed rate constants on the protein concentration. Unwinding rate constants were $k_{unw} = 0.015 \pm 0.002$ s^{-1} (*cis*) and $k_{unw} = 0.022 \pm 0.008$ s^{-1} (*trans*). The *cis*-like heterodimer showed a rate constant of RNA unwinding comparable to the *cis*-heterodimer ($k_{unw} = 0.012 \pm 0.003$ s^{-1}). The *trans*-like heterodimer had an unwinding rate constant of $k_{unw} = 0.009 \pm 0.002$ s^{-1}. These values are 3–7-fold lower than the rate constant of unwinding for Hera ($k_{unw} = 0.062 \pm 0.008$ s^{-1}), consistent with the reduced unwinding activity of a single helicase core.

The concentrations for half-maximal unwinding rates were $K_{1/2,unw} = 2.5 \pm 0.8$ μM (*cis*) or $K_{1/2,unw} = 8.7 \pm 3.9$ μM (*cis*-like), and $K_{1/2,unw} = 4 \pm 3.0$ μM (*trans*) or $K_{1/2,unw} = 2 \pm 1.1$ μM (*trans*-like). Although these values are affected by large errors, they indicate that, again, the *cis*-heterodimer (one core) behaved similar to wild-type (two cores). The *trans*-heterodimer is more similar to the dimeric core, reflecting the importance of the position of the RBD relative to the core for RNA binding. It is unclear why the *cis*-like and *trans*-like heterodimers are so different from the *cis*- and *trans*-dimers with respect to $K_{1/2,unw}$. It seems that the effect of the non-functional core present in *cis*- and *trans*-like heterodimers has opposite effects: less efficient interaction with RNA in the *cis*-like heterodimer compared to the *cis*-heterodimer, and more efficient interaction with RNA in the *trans*-like heterodimer compared to the *trans*-heterodimer.

ATP- and RNA-induced conformational changes: single-molecule FRET experiments

Finally, we also tested whether the relative position of the RBD toward the helicase core affects the ATP- and RNA-induced activation and closing of the (functional) helicase core (Fig. 7A). The *cis*-, *cis*-like, *trans*-, and *trans*-like heterodimers showed unimodal FRET histograms with $E_{FRET} \approx 0.5$. In the presence of RNA and ADPNP, all variants showed an increase in FRET efficiency, but to different extents. The mean FRET efficiencies of the high-FRET, closed states were similar, with $E_{FRET} = 0.65$–0.75. In all cases, the FRET efficiency of the high-FRET state increased with the concentration of the 32mer RNA, in agreement with the reduced RNA affinity of these heterodimers, indicating that saturation has not been reached yet (Fig. 7B). These data show that the helicase core can close independently of the relative position of (functional) core and RBD when ADPNP and RNA are present.

Collectively, we have shown that the RBD interacts predominantly with the helicase core of the same protomer in RNA binding, although RNA binding to the RBD of one pro-

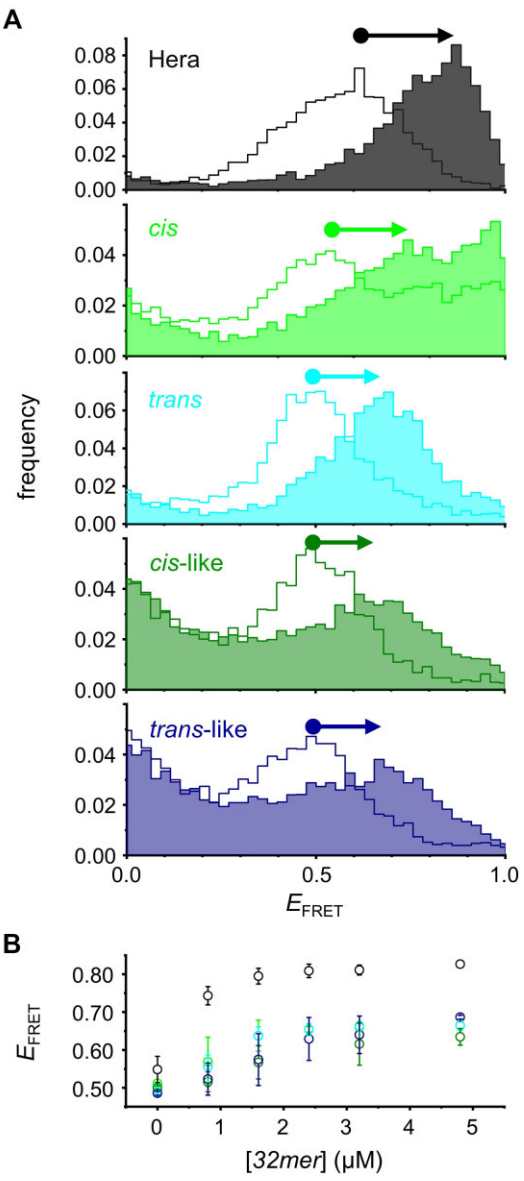

Figure 7. Cooperation of the helicase core(s) with the RBD(s): conformational changes of the helicase core. (**A**) Single-molecule FRET histograms for donor/acceptor-labeled Hera_E115C_E227C (black; same data as in Fig. 3A), Hera_E115C_E227C/Hera_208–419 (*cis*-heterodimer: one core, one RBD in *cis*; green), Hera_1–419_E115C_E227C/Hera_370–510 (*trans*-heterodimer: one core, one RBD in *trans*; cyan), Hera_E115C_E227C/Hera_1–419_K51Q (*cis*-like heterodimer: two cores, one functional core, RBD in *cis* to the functional core; dark green), and Hera_K51Q/Hera_1–419_E115C_E227C (*trans*-like heterodimer: two cores, one functional core, RBD in *trans* to the functional core; dark blue) in the absence (lines, no fill) and presence of 5 mM ADPNP and 4.8 μM of 32mer RNA (lines, colored fill). Representative histograms from at least two independent experiments. (**B**) FRET efficiency as a function of the 32mer concentration for donor/acceptor-labeled Hera_E115C_E227C (black; same data as in Fig. 3B), Hera_E115C_E227C/Hera_208–419 (*cis*-heterodimer; green), Hera_1–419_E115C_E227C/Hera_370–510 (*trans*-heterodimer; cyan), Hera_E115C_E227C/Hera_1–419_K51Q (*cis*-like heterodimer; dark green), and Hera_K51Q/Hera_1–419_E115C_E227C (*trans*-like heterodimer; dark blue) in the absence and presence of 5 mM ADPNP. Error bars are errors of the mean from at least two independent experiments.

tomer can facilitate interaction of the core on the opposite protomer with this RNA and induce core closing.

Discussion

Role of the RBDs and cores for RNA binding and unwinding

Here, we probed the contributions of the RBDs and the cores of the dimeric DEAD-box helicase Hera to RNA-stimulated ATPase activity, RNA binding, ATP-dependent RNA unwinding, and to closing of the helicase core in the presence of RNA and ATP.

RBDs

We show that RNA binds to Hera in a two-step mechanism, with an initial interaction between the C-terminal RBD and a hairpin, followed by the interaction of the core with the flanking single- or double-stranded region. While the Hera core shows little preference for single-stranded versus double-stranded RNA, it strongly prefers single-stranded RNA once the RNA is anchored to the RBD. The isolated RBD interacts more strongly with a hairpin flanked by single-stranded RNA, demonstrating that part of the preferential binding of Hera to a flanking single-stranded region stems from the RBD itself. The RBDs seem to play a role beyond RNA binding, however, and are also involved in the stimulation of ATP-hydrolysis by RNA and RNA unwinding. Interestingly, removing one of the two RBDs has only a moderate effect on RNA binding, but is sufficient to reduce the RNA-stimulated ATPase activity of Hera (per core) and the rate constant of RNA unwinding. Removing the second RBD strongly reduces the RNA affinity and has an additional deleterious effect on the unwinding activity but does not further compromise the ATPase activity of Hera. The conformational change in the helicase core of Hera on RNA and ATP binding that is necessary for RNA-stimulated ATP hydrolysis and ATP-dependent RNA unwinding can occur in the absence of the RBDs. These differential effects point to different levels of crosstalk and cooperativity within and between the protomers of the Hera dimer.

Cores

The effect of the Hera cores on the RNA-stimulated ATPase activity depends on the context: inactivating one of the cores in the Hera dimer has no effect on the ATPase activity or RNA affinity of the remaining functional core (Hera versus Hera/Hera_K51Q). Hera with only one core and one RBD also shows wildtype-like ATPase activity and RNA affinity (Hera versus the *cis*-heterodimer). Both observations suggest little cooperativity between the cores in ATP hydrolysis and RNA binding. However, in the absence of the RBDs (dimeric versus monomeric core), the number of cores does matter, both for ATP hydrolysis and for RNA binding, pointing to some cooperativity that may be masked in the presence of the RBD(s). In contrast, RNA unwinding shows (some) cooperativity between the two protomers both in the presence and absence of the RBDs: inactivating the core in one protomer (Hera versus Hera/Hera_K51Q) or removing one of the cores (dimeric versus monomeric core) both reduces the helicase activity of the remaining protomer. Consistent with these observations the unwinding activity of the *cis*-heterodimer is reduced compared to Hera. In contrast, RNA- and ATP-induced closing of the core is not only independent of the RBDs but also independent of the presence of the core in the second protomer.

Orientation of RBD and core

Hera with a single functional core and a single RBD in wildtype-like configuration (*cis*-heterodimer) can catalyze RNA-dependent ATP hydrolysis and binds single- and double-stranded RNA with wildtype-like properties. Despite this, the unwinding activity is reduced, consistent with some cooperativity between the protomers in the Hera dimer in unwinding. The orientation of the RBD with respect to the helicase core is critical for RNA binding: high-affinity RNA binding is achieved only if the RBD and the core are on the same protomer. If the RBD is located on the other protomer, RNA affinities resemble those of the isolated RBD. This picture changes in the presence of ATP, though: the RNA-stimulated ATPase activities of *cis*- and *trans*-heterodimers are similar, the conformational change of the helicase core is possible in both configurations, and the rate constants of RNA unwinding are similar. These observations show that the RBD on one protomer can functionally interact with the core on the other protomer, and suggest that ATP binding overrides the preference of the RBD to preferentially interact with the core in *cis*.

Comparison of Hera to other dimeric DEAD-box helicases

Hera is the founding member of a small sub-family of DEAD-box helicases that form stable dimers. Similar dimeric structures, formed by interactions between dimerization domains homologous to the one in Hera, have also been reported for *E. coli* CsdA/DeaD [29] and CshA from *Geobacillus stearothermophilus* [27]. Thus, dimeric DEAD-box helicases are not exclusive to thermophilic organisms, suggesting that dimerization is not predominantly a strategy to achieve thermostability, but may have functional implications. For both CsdA and CshA, some of the deletion variants corresponding to the ones we analyzed here for Hera have been characterized with respect to ATPase activity as well as RNA binding and unwinding [27, 29]. Strikingly, the affinities of CsdA, the dimeric core, and the isolated RBD for the 32mer (0.07, 28, and ~1 μM, respectively) are very similar to Hera. The RNA affinities of full-length CshA, the dimeric and the monomeric core, and the isolated RBD (0.31, 18, 6, and 0.30 μM for a hairpin RNA) are very similar to those of CsdA and of Hera, demonstrating that the RBD is the major binding platform and the anchor for CsdA, CshA, and Hera on RNA. The full-length protein shows the highest RNA affinity in all three helicases, demonstrating that RBD and core cooperate in RNA binding. In contrast to our observations with Hera, the monomeric core of CshA shows a higher affinity for RNA (6 μM) than the dimeric core (18 μM). CshA binds to a hairpin substrate in a 2:1 stoichiometry, with one dimer interacting with a single hairpin [27]. While the authors interpret this as a cooperation of both helicase cores in RNA unwinding, the underlying mechanism remains unclear.

The residues on the CsdA RBD involved in RNA binding differ from the ones that mediate RNA binding to Hera [21], suggesting different modes of binding even within this subfamily. Despite the different RNA binding modes, the CsdA RBD shows a preference for G-rich single-stranded RNAs similar to the GGGPur motif recognized by the Hera RBD [21].

Similar to Hera, the dimeric core of CsdA shows RNA-stimulated ATPase and ATP-dependent RNA unwinding activities, while no activity is detected for the monomeric core [29]. A CsdA deletion construct comprising the core, the DD, and the RRM of the RBD, but lacking the C-terminal tail, shows increased ATPase and RNA unwinding activities, suggesting that the RBDs of CsdA also contribute to these activities as we observe for Hera. For CshA, RNA-stimulated ATP hydrolysis was ~50-fold faster for the full-length protein compared to the dimeric and monomeric cores, suggesting a role of the RBD in RNA-stimulated ATP hydrolysis [27].

Cooperativity in other DEAD-box proteins

Beside the dimeric helicases CsdA and CshA, with an architecture similar to Hera, other DEAD-box helicases have been captured as dimers or functional multimers when bound to RNA. One example is the *E. coli* DEAD-box protein DbpA that has been crystallized in complex with an RNA substrate similar to the 32/9mer [44]. DpbA forms a dimer in the crystal, with the monomers cross-linked by the bound RNA. The relative arrangement of the two helicase cores in this dimer differs substantially from the relative orientation of the two cores in Hera (see Fig. 9B), and most likely does not have any functional relevance: previous work has shown that DbpA is a monomer over a wide range of conditions in solution [45]. In contrast, the *Saccharomyces cerevisiae* DEAD-box protein Ded1p has been described as a functional trimer, in which two "loading protomers" bind to single-stranded regions and recruit a third protomer that catalyzes unwinding of an adjacent duplex [46]. A similar multimerization, induced by the RNA substrate, has been suggested for eIF4A [47]. Structural studies of the human ortholog of Ded1p, DDX3X, bound to double-stranded RNA, revealed two helicase molecules, each interacting with one of the two strands of the same duplex [48] (see Fig. 9A). This arrangement has been interpreted as cooperative action of the two helicase cores on duplex destabilization. Again, the relative geometry of the two monomers is very different from the juxtaposition of the two helicase cores in Hera, suggesting different modes of action.

A structural model for the interaction of Hera with RNA?

How can the cooperation between RBD and core in RNA binding be rationalized on a structural level? The crystal structure of the RBD of *B. subtilis* YxiN [49] with an RNA containing hairpin 92 of the 23S RNA has revealed the molecular details of the interaction of this RBD with hairpin 92 in the 32mer and 32/9mer (Fig. 8A), with interactions between conserved residues of the RBD and bases in the apical loop of hairpin 92. A very similar binding mode was observed for *E. coli* DbpA [44] (Fig. 8A). The RBD of Hera is structurally distinct from the RBDs of YxiN and DbpA [17], and RNA binding to the RBD of Hera is markedly different [21]. Binding of RNA to Hera is mediated by a different interface and set of RBD residues, leading to a binding site with different specificity [21]. The position of single-stranded RNA bound to the Hera RBD is different from the position of the loop bound to YxiN and DbpA (Fig. 8A). In fact, the Hera RBD does not recognize the loop, but instead interacts with a flanking single-stranded region through the RRM and with the stem of the hairpin though its C-terminal tail [21], which is reflected in

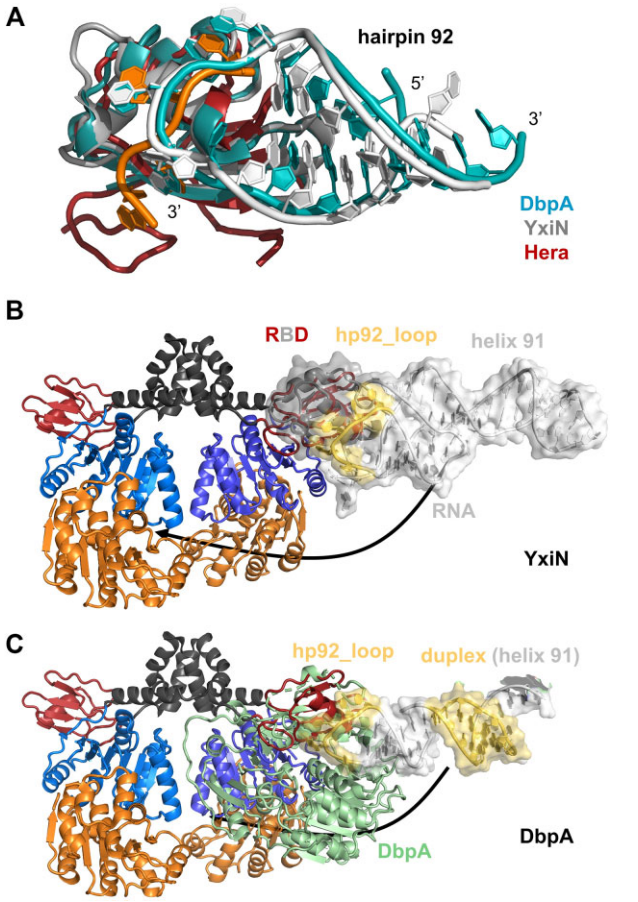

Figure 8. RNA binding to the RBDs of Hera and other DEAD-box proteins. (**A**) Superposition of the structures of the *B. subtilis* YxiN RBD (gray) in complex with a 74mer derived from nucleotides 2508–2580 of *E. coli* 23S rRNA (white; PDB ID: 3moj; only hairpin 92 bound to the RBD is shown) and *E. coli* DbpA (dark teal) in complex with a 44mer RNA derived from nucleotides 2520–2562 of *E. coli* 23S rRNA (teal; PDB ID: 7pmm; only hairpin 92 bound to the RBD is shown) with the Hera RBD (red) in complex with a single-stranded GGGC 4mer RNA (orange; PBD ID: 4i67). The conformation and position of the RNA bound to the Hera RBD is different from the loop region recognized by YxiN and DbpA. (**B**) Structural model for full-length Hera (orange: RecA_N, blue: RecA_C, dark gray: DD, red: RBD; see Fig. 1B) with the RNA-bound YxiN RBD (gray/white) superimposed on the Hera RBD. The loop of hairpin 92 recognized by the YxiN RBD is highlighted in yellow. (**C**) Structural model for full-length Hera (see Fig. 1B) with the RNA-bound DbpA RBD (pale green, white) superimposed on the Hera RBD. The loop of hairpin 92 recognized by the DbpA RBD and the duplex in helix 91 that corresponds to the duplex unwound in the 32/9mer are highlighted in yellow.

the higher affinity of the RBD for the 32mer compared to the 32/9mer, as we report here.

In the structures of the RNA complexes of YxiN and DbpA, the duplex region that is unwound by the helicase core points away from the core (Fig. 8B and C), implying a substantial conformational change before unwinding can occur. Although single-molecule FRET experiments revealed a conformational change of YxiN on RNA binding to the RBD, involving a large translational and rotational motion of the RBD relative to the YxiN core that leads to its allosteric activation [50], there is no supporting evidence for such a motion of the RBD on RNA binding in DpbA [51].

The possible position of a duplex bound to the Hera helicase core can be gleaned from structural information on the

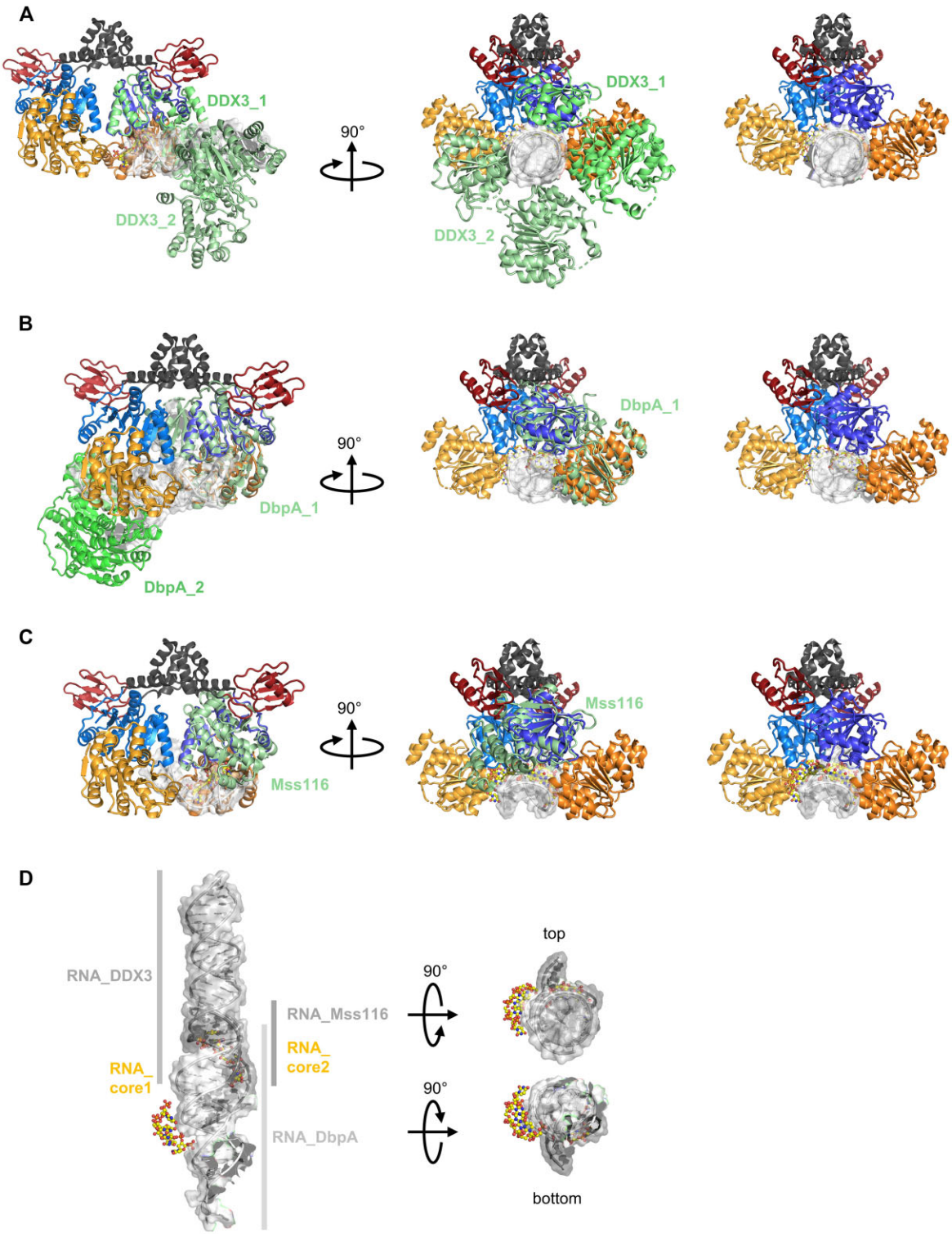

Figure 9. Duplex RNA binding to the helicase core of DEAD-box proteins. (**A**) Left: Front and side view of the superposition of the structures of DDX3X (pale green/green) in complex with an RNA duplex (white; PDB ID: 7pmm) with the Hera RecA_C (blue). DDX3_1: molecule 1, DDX3_2: molecule 2, bound to the same duplex. Right: Side-view without DDX3 showing the position of the duplex between the two helicase cores of Hera. Yellow: RNA as bound to the helicase core of Vasa (PDB ID: 2db3). (**B**) Left: Front and side view of the superposition of the structures of DbpA (pale green/green) in complex with an RNA duplex (white; PDB ID: 7pmm) with the Hera RecA_C (blue). DbpA_1: molecule 1, DbpA_2: molecule 2. Right: side-view without DbpA showing the position of the duplex between the two helicase cores of Hera. Yellow: RNA as bound to the helicase core of Vasa, superimposed on the Hera cores (PDB ID: 2db3), marking the active site of the two helicase cores of Hera. (**C**) Left: Front and side view of the superposition of the structures of Mss116 (pale green) in complex with an RNA duplex (white; PDB ID: 4db2) with the Hera RecA_C (blue). Right: side-view without Mss116. Yellow: RNA as bound to the helicase core of Vasa, superimposed on the Hera cores (PDB ID: 2db3), marking the active site of the two helicase cores of Hera. (**D**) Superposition of the duplex RNAs bound to DDX3X, DbpA, and Mss116 in panels (A–C), and position of the two single-stranded RNAs marking the active sites of the helicase core in Hera. Left: Bottom view (relative to the depiction in panels A–C), right: top and bottom view with respect to depiction on the left.

helicase cores of DbpA [44], the DEAD-box helicase DDX3 [48], and Mss116 [52] bound to RNA duplexes. Superposition of these cores with one of the helicase cores of Hera (Fig. 9A–C) places the RNA duplex between the two helicase cores, with the backbone of one of the strands superimposing closely with the single-stranded RNA as bound to the helicase core of Vasa [23]. The RNA binding site on the second core of Hera is barely 10 Å away (Fig. 9D), demonstrating that only a small conformational change of the dimer would enable cooperative action of both cores on the same duplex. Such a binding mode would suggest a stoichiometry of one RNA bound per Hera dimer, which has been observed for binding of an RNA hairpin to the dimeric helicase CshA [27].

In the structure of the DbpA dimer, each RNA binds to the RBD of one DbpA molecule via hairpin 92, and to the helicase core of the other DbpA molecule through the duplex region. The distance between the hairpin of one RNA bound to the RBD and of the duplex of the second RNA molecule bound to the core of the same DbpA molecule can be bridged by the three nucleotides connecting hairpin and duplex in the RNA substrate, affording a molecular model of 32/9mer binding to DbpA [51] (Supplementary Fig. S12). The RBD in Hera has a very different position relative to the helicase core in Hera compared to DbpA and YxiN, and interacts with the stem of hairpin 92 and the 5′-sequence flanking the hairpin 92 instead of the apical loop. Constructing a model for the 32/9mer bound to Hera is not as straightforward as for DbpA (Supplementary Fig. S12). The two ends of RNA that are covalently linked in the 32mer, the 5′-end of the RNA bound at the RBD and the 3′-end of the duplex strand superimposing with the single-stranded RNA as bound to the helicase core of Vasa, are 58 Å apart. Although the distance between the 5′-end of the RNA bound at the RBD in the opposite protomer is much smaller, 36 Å, it is still much too large for a covalent linkage without any conformational change. The molecular details of the interactions of the Hera domains with RNA will only be unraveled by structural data for a Hera–RNA complex.

Conclusions

From our data, a picture emerges in which Hera binds RNAs through its RBD that serves as an anchor point and enables the helicase core to unwind adjacent duplexes. If the duplex to be unwound is placed at the active site of one helicase core in such a way that the second helicase core would have to move just a few Ångstrom to act on the same duplex, both cores could act cooperatively in unwinding of this duplex. Notably, the juxtaposition of the two helicase cores in Hera is such that they would act on the same strand of the duplex, not on opposite strands as in the DDX3X–RNA complex. Such a mode of action would actually be more efficient as it enables the two protomers to destabilize a longer duplex region. It would also explain why deletion of one RBD in Hera is not as deleterious as deleting both RBDs: one RBD would be sufficient to facilitate binding of the helicase core to an adjacent duplex, and the second core is always within close reach. It would further rationalize the activities of the *cis*- and *trans* heterodimers: in both cases, the single RBD initiates RNA binding, facilitating the interaction of the helicase core with the duplex. The intrinsic plasticity of the DD enables changes in the relative orientation of the RBD and the two helicase cores. Unwinding with a single core is less efficient, which could be linked to the destabilization of a shorter region of the duplex by the action of a single core. The presence of two RBDs in the Hera dimer might constitute an additional benefit and make the capture of RNAs for unwinding more efficient. Altogether, the Hera dimer thus might be optimized for efficient unwinding of RNA substrates by the concerted action of two cores.

Acknowledgements

We thank Jochen Reinstein for helpful discussions, Christoph Flüchter for preliminary experiments with Hera containing two helicase cores and a single RBD, and Jessica Guddorf and Daniela Schlingmeier for excellent technical assistance.

Author contributions: D.K. conceptualized research and acquired funding. P.D., C.K., L.S., B.S., and A.Z.Z. performed experiments. P.D., B.S., A.Z.Z., and D.K. designed experiments. P.D., C.K., B.S., A.Z.Z., and D.K. analyzed data. P.D. and D.K. wrote and revised the manuscript.

Supplementary data

Supplementary data is available at NAR online.

Conflict of interest

None declared.

Funding

This work was supported by the Deutsche Forschungsgemeinschaft (DFG) (KL1153/7-1, 7-2 to D.K.). Funding to pay the Open Access publication charges for this article was provided by the University of Muenster.

Data availability

All data described are presented in the manuscript figures and/or tables, or in the Supplementary data. Original data are available from the corresponding author on request.

References

1. Donsbach P, Klostermeier D. Regulation of RNA helicase activity: principles and examples. *Nature* 2021;**402**:121–25. https://doi.org/10.1515/hsz-2020-0362
2. Linder P, Jankowsky E. From unwinding to clamping—the DEAD box RNA helicase family. *Nat Rev Mol Cell Biol* 2011;**12**:505–16. https://doi.org/10.1038/nrm3154
3. Hilbert M, Karow AR, Klostermeier D. The mechanism of ATP-dependent RNA unwinding by DEAD box proteins. *Biol Chem* 2009;**390**:1237–50. https://doi.org/10.1515/BC.2009.135
4. Collins R, Karlberg T, Lehtio L *et al.* The DExD/H-box RNA helicase DDX19 is regulated by an alpha-helical switch. *J Biol Chem* 2009;**284**:10296–300. https://doi.org/10.1074/jbc.C900018200
5. Fan JS, Cheng Z, Zhang J *et al.* Solution and crystal structures of mRNA exporter Dbp5p and its interaction with nucleotides. *J Mol Biol* 2009;**388**:1–10. https://doi.org/10.1016/j.jmb.2009.03.004
6. Napetschnig J, Kassube SA, Debler EW *et al.* Structural and functional analysis of the interaction between the nucleoporin Nup214 and the DEAD-box helicase Ddx19. *Proc Natl Acad Sci USA* 2009;**106**:3089–94. https://doi.org/10.1073/pnas.0813267106

7. von Moeller H, Basquin C, Conti E. The mRNA export protein DBP5 binds RNA and the cytoplasmic nucleoporin NUP214 in a mutually exclusive manner. *Nat Struct Mol Biol* 2009;**16**:247–54. https://doi.org/10.1038/nsmb.1561
8. Linden MH, Hartmann RK, Klostermeier D. The putative RNase P motif in the DEAD box helicase Hera is dispensable for efficient interaction with RNA and helicase activity. *Nucleic Acids Res* 2008;**36**:5800–11. https://doi.org/10.1093/nar/gkn581
9. Yan X, Mouillet JF, Ou Q *et al.* A novel domain within the DEAD-box protein DP103 is essential for transcriptional repression and helicase activity. *Mol Cell Biol* 2003;**23**:414–23. https://doi.org/10.1128/MCB.23.1.414-423.2003
10. Pugh GE, Nicol SM, Fuller-Pace FV. Interaction of the *Escherichia coli* DEAD box protein DbpA with 23 S ribosomal RNA. *J Mol Biol* 1999;**292**:771–78. https://doi.org/10.1006/jmbi.1999.3112
11. Karginov FV, Caruthers JM, Hu Y *et al.* YxiN is a modular protein combining a DEx(D/H) core and a specific RNA-binding domain. *J Biol Chem* 2005;**280**:35499–505. https://doi.org/10.1074/jbc.M506815200
12. Kossen K, Karginov FV, Uhlenbeck OC. The carboxy-terminal domain of the DExDH protein YxiN is sufficient to confer specificity for 23S rRNA. *J Mol Biol* 2002;**324**:625–36. https://doi.org/10.1016/S0022-2836(02)01140-3
13. Tijerina P, Bhaskaran H, Russell R. Nonspecific binding to structured RNA and preferential unwinding of an exposed helix by the CYT-19 protein, a DEAD-box RNA chaperone. *Proc Natl Acad Sci USA* 2006;**103**:16698–703. https://doi.org/10.1073/pnas.0603127103
14. Del Campo M, Lambowitz AM. Structure of the yeast DEAD-box protein Mss116p reveals two wedges that crimp RNA. *Mol Cell* 2009;**35**:598–609. https://doi.org/10.1016/j.molcel.2009.07.032
15. Morlang S, Weglohner W, Franceschi F. Hera from *Thermus thermophilus*: the first thermostable DEAD-box helicase with an RNase P protein motif. *J Mol Biol* 1999;**294**:795–805. https://doi.org/10.1006/jmbi.1999.3282
16. Klostermeier D. Rearranging RNA structures at 75°C? Towards the molecular mechanism and physiological function of the *Thermus thermophilus* DEAD-box helicase Hera. *Biopolymers* 2013;**99**:1137–46. https://doi.org/10.1002/bip.22316
17. Rudolph MG, Klostermeier D. The *Thermus thermophilus* DEAD box helicase Hera contains a modified RNA recognition motif domain loosely connected to the helicase core. *RNA* 2009;**15**:1993–2001. https://doi.org/10.1261/rna.1820009
18. Rudolph MG, Wittmann JG, Klostermeier D. Crystallization and preliminary characterization of the *Thermus thermophilus* RNA helicase Hera C-terminal domain. *Acta Crystallogr. Sect. F* 2009;**65**:248–52. https://doi.org/10.1107/S1744309108043145
19. Klostermeier D, Rudolph MG. A novel dimerization motif in the C-terminal domain of the *Thermus thermophilus* DEAD box helicase Hera confers substantial flexibility. *Nucleic Acids Res* 2009;**37**:421–30. https://doi.org/10.1093/nar/gkn947
20. Rudolph MG, Heissmann R, Wittmann JG *et al.* Crystal structure and nucleotide binding of the *Thermus thermophilus* RNA helicase Hera N-terminal domain. *J Mol Biol* 2006;**361**:731–43. https://doi.org/10.1016/j.jmb.2006.06.065
21. Steimer L, Wurm JP, Linden MH *et al.* Recognition of two distinct elements in the RNA substrate by the RNA binding domain of the *T. thermophilus* DEAD box helicase Hera. *Nucleic Acids Res* 2013;**41**:6259–72. https://doi.org/10.1093/nar/gkt323
22. Donsbach P, Yee BA, Sanchez-Hevia D *et al.* The *Thermus thermophilus* DEAD-box protein Hera is a general RNA binding protein and plays a key role in tRNA metabolism. RNA 2020;**26**:1557–74. https://doi.org/10.1261/rna.075580.120
23. Sengoku T, Nureki O, Nakamura A *et al.* Structural basis for RNA unwinding by the DEAD-box protein *Drosophila* vasa. *Cell* 2006;**125**:287–300. https://doi.org/10.1016/j.cell.2006.01.054
24. Polach KJ, Uhlenbeck OC. Cooperative binding of ATP and RNA substrates to the DEAD/H protein DbpA. *Biochemistry* 2002;**41**:3693–702. https://doi.org/10.1021/bi012062n
25. Wang S, Hu Y, Overgaard MT *et al.* The domain of the *Bacillus subtilis* DEAD-box helicase YxiN that is responsible for specific binding of 23S rRNA has an RNA recognition motif fold. *RNA* 2006;**12**:959–67. https://doi.org/10.1261/rna.5906
26. Kossen K, Uhlenbeck OC. Cloning and biochemical characterization of *Bacillus subtilis* YxiN, a DEAD protein specifically activated by 23S rRNA: delineation of a novel sub-family of bacterial DEAD proteins. *Nucleic Acids Res* 1999;**27**:3811–20. https://doi.org/10.1093/nar/27.19.3811
27. Huen J, Lin CL, Golzarroshan B *et al.* Structural insights into a unique dimeric DEAD-box helicase CshA that promotes RNA decay. *Structure* 2017;**25**:469–81. https://doi.org/10.1016/j.str.2017.01.012
28. Stampfl S, Doetsch M, Beich-Frandsen M *et al.* Characterization of the kinetics of RNA annealing and strand displacement activities of the *E. coli* DEAD-box helicase CsdA. *RNA Biol* 2013;**10**:149–56. https://doi.org/10.4161/rna.23475
29. Xu L, Wang L, Peng J *et al.* Insights into the structure of dimeric RNA helicase CsdA and indispensable role of its C-terminal regions. *Structure* 2017;**25**:1795–808. https://doi.org/10.1016/j.str.2017.09.013
30. Peil L, Virumae K, Remme J. Ribosome assembly in *Escherichia coli* strains lacking the RNA helicase DeaD/CsdA or DbpA. *FEBS J* 2008;**275**:3772–82. https://doi.org/10.1111/j.1742-4658.2008.06523.x
31. Charollais J, Dreyfus M, Iost I. CsdA, a cold-shock RNA helicase from *Escherichia coli*, is involved in the biogenesis of 50S ribosomal subunit. *Nucleic Acids Res* 2004;**32**:2751–59. https://doi.org/10.1093/nar/gkh603
32. Khemici V, Prados J, Petrignani B *et al.* The DEAD-box RNA helicase CshA is required for fatty acid homeostasis in *Staphylococcus aureus*. *PLoS Genet* 2020;**16**:e1008779. https://doi.org/10.1371/journal.pgen.1008779
33. Oun S, Redder P, Didier JP *et al.* The CshA DEAD-box RNA helicase is important for quorum sensing control in *Staphylococcus aureus*. *RNA Biol* 2012;**10**:157–65. https://doi.org/10.4161/rna.22899
34. Hunger K, Beckering CL, Wiegeshoff F *et al.* Cold-induced putative DEAD box RNA helicases CshA and CshB are essential for cold adaptation and interact with cold shock protein B in *Bacillus subtilis*. *J Bacteriol* 2006;**188**:240–48. https://doi.org/10.1128/JB.188.1.240-248.2006
35. Francais M, Carlin F, Broussolle V *et al. Bacillus cereus* CshA is expressed during the lag-phase and serves as a potential marker of early adaptation to low temperature and pH. *Appl Environ Microb* 2019;**85**:e00486-19. https://doi.org/10.1128/AEM.00486-19
36. Palonen E, Lindstrom M, Somervuo P *et al.* Requirement for RNA helicase CsdA for growth of *Yersinia pseudotuberculosis* IP32953 at low temperatures. *Appl Environ Microb* 2012;**78**:1298–301. https://doi.org/10.1128/AEM.07278-11
37. Awano N, Xu C, Ke H *et al.* Complementation analysis of the cold-sensitive phenotype of the *Escherichia coli* CsdA deletion strain. *J Bacteriol* 2007;**189**:5808–15. https://doi.org/10.1128/JB.00655-07
38. Gasteiger E, Hoogland C, Gattiker A *et al.* Protein identification and analysis tools on the ExPASy server. In: Walker JM (ed.), *The Proteomics Protocols Handbook*. Humana Press, 2005, 571–607.
39. Studier FW. Protein production by auto-induction in high density shaking cultures. *Protein Expr Purif* 2005;**41**:207–34. https://doi.org/10.1016/j.pep.2005.01.016
40. Adam H. *Methoden der Enzymatischen Analyse*. Weinheim: Bergmeyer, H.U.(Hrsg.), Verlag Chemie, 1962, 573–77.
41. Kuzmic P. DynaFit–a software package for enzymology. *Methods Enzymol* 2009;**467**:247–80. https://doi.org/10.1016/S0076-6879(09)67010-5
42. Kuzmic P. Program DYNAFIT for the analysis of enzyme kinetic data: application to HIV proteinase. *Anal Biochem* 1996;**237**:260–73. https://doi.org/10.1006/abio.1996.0238

43. Andreou AZ, Klostermeier D. Conformational changes of DEAD-box helicases monitored by single molecule fluorescence resonance energy transfer. *Methods Enzymol* 2012;**511**:75–109. https://doi.org/10.1016/B978-0-12-396546-2.00004-8
44. Wurm JP. Structural basis for RNA-duplex unwinding by the DEAD-box helicase DbpA. *RNA* 2023;**29**:1339–54. https://doi.org/10.1261/rna.079582.123
45. Talavera MA, Matthews EE, Eliason WK *et al.* Hydrodynamic characterization of the DEAD-box RNA helicase DbpA. *J Mol Biol* 2006;**355**:697–707. https://doi.org/10.1016/j.jmb.2005.10.058
46. Putnam AA, Gao Z, Liu F *et al.* Division of labor in an oligomer of the DEAD-box RNA helicase Ded1p. *Mol Cell* 2015;**59**:541–52. https://doi.org/10.1016/j.molcel.2015.06.030
47. Schmidt T, Dabrowska A, Waldron JA *et al.* eIF4A1-dependent mRNAs employ purine-rich 5′UTR sequences to activate localised eIF4A1-unwinding through eIF4A1-multimerisation to facilitate translation. *Nucleic Acids Res* 2023;**51**:1859–79. https://doi.org/10.1093/nar/gkad030
48. Song H, Ji X. The mechanism of RNA duplex recognition and unwinding by DEAD-box helicase DDX3X. *Nat Commun* 2019;**10**:3085. https://doi.org/10.1038/s41467-019-11083-2
49. Hardin JW, Hu YX, McKay DB. Structure of the RNA binding domain of a DEAD-box helicase bound to its ribosomal RNA target reveals a novel mode of recognition by an RNA recognition motif. *J Mol Biol* 2010;**402**:412–27. https://doi.org/10.1016/j.jmb.2010.07.040
50. Samatanga B, Andreou AZ, Klostermeier D. Allosteric regulation of helicase core activities of the DEAD-box helicase YxiN by RNA binding to its RNA recognition motif. *Nucleic Acids Res* 2017;**45**:1994–2006.
51. Wurm JP, Glowacz KA, Sprangers R. Structural basis for the activation of the DEAD-box RNA helicase DbpA by the nascent ribosome. *Proc Natl Acad Sci USA* 2021;**118**:e2105961118. https://doi.org/10.1073/pnas.2105961118
52. Mallam AL, Del Campo M, Gilman B *et al.* Structural basis for RNA-duplex recognition and unwinding by the DEAD-box helicase Mss116p. *Nature* 2012;**490**:121–25. https://doi.org/10.1038/nature11402

Received: August 29, 2024. **Revised:** January 20, 2025. **Editorial Decision:** January 24, 2025. **Accepted:** February 3, 2025